IC/97/61

INTERNATIONAL CENTRE FOR THEORETICAL PHYSICS

COHERENT TUNNELING OF BOSE-EINSTEIN CONDENSATES: EXACT SOLUTIONS FOR JOSEPHSON EFFECTS AND MACROSCOPIC QUANTUM SELF-TRAPPING

S. Raghavan

A. Smerzi

S. Fantoni

and

S.R. Shenoy

MIRAMARE-TRIESTE

VOL. 28 № 23

IC/97/61

United Nations Educational Scientific and Cultural Organization
and
International Atomic Energy Agency
INTERNATIONAL CENTRE FOR THEORETICAL PHYSICS

COHERENT TUNNELING OF BOSE-EINSTEIN CONDENSATES: EXACT SOLUTIONS FOR JOSEPHSON EFFECTS AND MACROSCOPIC QUANTUM SELF-TRAPPING

S. Raghavan
International Centre for Theoretical Physics, Trieste, Italy,

A. Smerzi
International School for Advanced Studies, Trieste, Italy,

S. Fantoni
International Centre for Theoretical Physics, Trieste, Italy
and
International Centre for Theoretical Physics, Trieste, Italy

and

S.R. Shenoy
International Centre for Theoretical Physics, Trieste, Italy.

MIRAMARE - TRIESTE
July 1997

ABSTRACT

We consider coherent atomic tunneling between two weakly coupled Bose-Einstein condensates (BEC) at T=0 in (possibly asymmetric) double-well trap. The condensate dynamics of the macroscopic amplitudes in the two wells is modeled by two Gross-Pitaevskii equations (GPE) coupled by a tunneling matrix element. The evolution of the inter-well fractional population imbalance (related to the condensate phase difference) is obtained in terms of elliptic functions, generalizing well-known Josephson effects such as the 'ac' effect, the 'plasma oscillations', and the resonant Shapiro effect, to nonsinusoidal regimes. We also present exact solutions for a novel 'macroscopic quantum self-trapping' effect arising from nonlinear atomic self-interaction in the GPE. The coherent BEC tunneling signatures are obtained in terms of the oscillation periods and the Fourier spectrum of the imbalance oscillations, as a function of the initial values of GPE parameters. Experimental procedures are suggested to make contact with theoretical predictions.

I. INTRODUCTION

Bose-Einstein condensation, predicted some 70 years ago [1,2], was detected in 1995, in alkali atoms held in magnetic traps, where a non-thermal velocity distribution below a $\sim$170nK transition temperature signaled macroscopic condensation into a single quantum state [3–5]. The existence of a quantum phase of the macroscopic wave function was demonstrated by dividing a magnetic trap into two condensates by a far off-resonant laser. On switching off the confining traps and barrier, the condensates, of different phases, overlapped, producing robust interference fringes [6]. The *non*-destructive detection of a coherent phase difference could be implemented by ac Bose-condensate analogs of Josephson effects that occur in superconductor Josephson junctions (SJJ) [7],or other phase coherent oscillations [8].

The macroscopic wavefunction of N condensate atoms $\Psi(r,t)$ of a Bose condensate in a trap obeys the Gross-Pitaevskii equation (GPE) [9]. The GPE has been applied to study the collective mode frequencies of a trapped BEC [10,11], the relaxation times of monopolar oscillations [12], and chaotic behavior in dynamical quantum observables [12,13]. For two Bose condensates in a double-well trap with N_1, N_2 atoms, one can write down wavefunctions that have their spatial variation described by the isolated trap eigenstates $\Phi_{1,2}(r)$ and their time-dependence by amplitudes $\psi_{1,2}(t) = \sqrt{N_{1,2}(t)}e^{i\theta_{1,2}(t)}$. These amplitudes also obey two GPE-like equations coupled by a tunneling matrix element between the two traps [14], with spatial variation integrated out into constant GPE parameters. The tunneling dynamics can be written in terms of the fractional population difference $z(t) \equiv (N_1(t) - N_2(t))/N_T$, where $N_T = N_1 + N_2$, a constant; and the relative phase $\phi(t) \equiv \theta_1(t) - \theta_2(t)$. Predictions for $z(t), \phi(t)$ oscillations have been made from numerical solutions of the tunneling dynamical equations for $z(t), \phi(t)$ [14]. As we suggested earlier, [14], the ability to tailor traps, and the non-ideal nature of the BEC should, remarkably, make the (neutral atom) double-well BEC closer to the charged-pair SJJ than to neutral-atom HeII, and lead to Josephson-lke effects in a Bose system. Non-sinusoidal *generalizations* of the familiar [7] sinusoidal Josephson effects in SJJ emerge, including the 'plasma' or population imbalance oscillations (for symmetric traps); the 'ac' effect (for asymmetric traps); and the resonant Shapiro effect (for asymmetric traps with imposed trap/barrier oscillations). In addition, and as a consequence of the nonlinear atomic self-interaction of the nonideal Bose gas, a novel 'macroscopic quantum self-trapping' (MQST) effect was predicted [14] with population oscillations around a self-

maintained imbalance, beyond a critical value $\Lambda_c(z(0),\phi(0))$ of the ratio $\Lambda \equiv UN_T/2\mathcal{K}$ of the self-interaction to the tunneling matrix element. Mechanical analogs, e.g., in terms of a *non-rigid* pendulum, clarify the rich dynamical behavior. Experimental detection of predicted effects could be through temporal modulations (of the order of milliseconds) of phase-contrast fringes [6] or other probes of atomic populations [3], with integrated signal $\sim z(t)$. Oscillating currents $\dot{z}(t)$ might be monitored by Doppler interferometry methods.

The nonlinear GPE tunnelling equations for the macroscopic amplitudes $\psi_1(t), \psi_2(t)$ are formally identical to equations governing a physically very different problem — a single electron in a polarizable medium, forming a polaron [15]. Exact solutions have been found [15], for the discrete nonlinear Schrödinger equation (DNLSE) describing the motion of the polaron between two sites of a dimer.

This paper is an extension of our previous work [14], presenting exact solutions that apply to BEC tunneling between two symmetric wells. The fractional population imbalance $z(t)$ (and the related phase difference $\phi(t)$) can be written in terms of Jacobian or Weierstrassian elliptic functions for symmetric and asymmetric well cases. (These reduce to sinusoidal SJJ dependences in the linearized, noninteracting Bose gas limit.) The period of the non-sinusoidal oscillations is obtained in terms of the tunneling and other double-well parameters and total atomic densities. The frequency spectrum, with harmonics of these basic frequencies, is also obtained. Just at $\Lambda = \Lambda_c$, the onset of MQST, there is a 'critical slowing down', with a simplified analytic form governing the relaxation of $\langle z(t)\rangle$ to its nonzero asymptotic value. Thus, the predicted Josephson effect generalizations and MQST effects are obtained as exact elliptic functional predictions, that can be experimentally tested.

The plan of the paper is as follows: In Section II (and Appendix A), we obtain the coupled GPE tunneling equations for $z(t), \phi(t)$, and discuss the varied oscillations in terms of mechanical analogs, pointing out similarities and differences with SJJ. In Section III, we cast the GPE equations in terms of imbalance $z(t)$, and variables $i(t), e(t)$ related to the Josephson tunneling current and coupling energy respectively. For the symmetric well case, the exact solutions for $z(t)$ follow immediately in terms of Jacobian elliptic functions. The time-period $\tau(\Lambda, z(0), \phi(0))$ and Fourier spectrum $z(\omega)$ are also obtained. The generalized Josephson plasma oscillation and the MQST effect and its onset are discussed. In Section IV, we consider the (static) asymmetric double well, with the 'ac Josephson effect' and $z(t)$ oscillation expressed in terms of Weierstrassian elliptic functions. The analog of the Shapiro resonance is considered in Section V, with an imposed incremental oscillation in the tunneling

matrix element. Finally, we suggest possible experimental procedures to set up various initial conditions/parameter regimes and summarize our results in Section VI. For completeness, Appendix B contains an outline of elliptic function properties and relations.

II. TUNNELING DYNAMICS EQUATIONS

The BEC wavefunction $\Psi(r,t)$ in a single trap potential $V_{ext}(r,t)$ is known to satisfy the Gross-Pitaevskii equation [9] at $T=0$ (with derivation and possible $T\neq 0$ corrections sketched in Appendix A),

$$i\hbar\frac{d\Psi(r,t)}{dt}=-\frac{\hbar^2}{2m}\nabla^2\Psi(r,t)+[V_{ext}(r)+g_0|\Psi(r,t)|^2]\Psi(r,t), \tag{2.1}$$

$g_0=4\pi\hbar^2a/m$, and a is the scattering length of the atoms. Consider a double-well trap, produced by a laser barrier [6], with isolated well GPE (normalized) eigenfunctions $\Phi_{1,2}(r)$ in wells $1,2$, of equal occupations $N_T/2=N_1=N_2$, with eigenvalues, $E_{1,2}$,

$$E_{1,2}\Phi_{1,2}(r)=-\frac{\hbar^2}{2m}\nabla^2\Phi_{1,2}(r)+[V_{ext}(r)+g_0\frac{N_T}{2}|\Phi_{1,2}(r)|^2]\Phi_{1,2}(r). \tag{2.2}$$

The amplitudes

$$\psi_{1,2}(t)=\sqrt{N_{1,2}}e^{i\theta_{1,2}(t)} \tag{2.3}$$

with general occupations $N_{1,2}(t)$ and phases $\theta_{1,2}(t)$, now including the inter-well tunneling, obey the dynamical equations [14],

$$i\hbar\frac{\partial\psi_1}{\partial t}=(E_1^0+U_1N_1)\psi_1-\mathcal{K}\psi_2 \tag{2.4a}$$

$$i\hbar\frac{\partial\psi_2}{\partial t}=(E_2^0+U_2N_2)\psi_2-\mathcal{K}\psi_1, \tag{2.4b}$$

where $E_{1,2}^0$ are the zero-point energies in each well (that could be different for asymmetric wells), $U_{1,2}N_{1,2}$ are the atomic self-interaction energies, and $\mathcal{K}$ describes the amplitude of the tunneling between condensates [14]. See Fig. 1. The parameters $E_{1,2}^0, U_{1,2}, \mathcal{K}$ can be written in terms of $\Phi_{1,2}(r)$ wave-function overlaps with the potential and kinetic energy contributions, as in Appendix A. The total number of atoms, $N_1+N_2=|\psi_1|^2+|\psi_2|^2=N_T$ is a constant. The fractional population imbalance

$$z(t)\equiv(N_1(t)-N_2(t))/N_T\equiv(|\psi_1|^2-|\psi_2|^2)/N_T \tag{2.5}$$

and relative phase

$$\phi(t) \equiv \theta_2(t) - \theta_1(t) \tag{2.6}$$

obey

$$\dot{z}(t) = -\sqrt{1-z^2(t)}\sin(\phi(t)), \tag{2.7a}$$

$$\dot{\phi}(t) = \Delta E + \Lambda z(t) + \frac{z(t)}{\sqrt{1-z^2(t)}}\cos(\phi(t)), \tag{2.7b}$$

where

$$\Delta E \equiv (E_1^0 - E_2^0)/2\mathcal{K} + (U_1 - U_2)/2\mathcal{K}, \tag{2.8a}$$

$$\Lambda \equiv UN_T/2\mathcal{K}\ ;\ U \equiv (U_1 + U_2)/2, \tag{2.8b}$$

and we have rescaled to a dimensionless time, $t2\mathcal{K}/\hbar \rightarrow t$. There must be a minimum population $N_{1,2} \geq N_{min}$, so phase fluctuations [16,17] $\sim 1/\sqrt{N_{min}}$ are small and phase differences are stiff. For $\sim 3\%$ errors, we take $N_{min} \sim 10^3$ atoms and have $|z| \lesssim |1 - 2N_{min}/N_T|$, that can be satisfied. The tunneling current I, and a scaled current $i \equiv I/(N_T/2)$ are given by

$$I = \dot{N}_1 - \dot{N}_2 \equiv |\dot{\psi_1}|^2 - |\dot{\psi_2}|^2 = \frac{N_T}{2}\dot{z} = -\frac{N_T}{2}\sqrt{1-z^2}\sin\phi \equiv \frac{N_T}{2}i(t). \tag{2.9}$$

The coupling energy W and a scaled energy $w \equiv W/(N_T/2)$ are given by

$$W = \frac{\psi_1\psi_2^* + \psi_1^*\psi_2}{2} = -\frac{N_T}{2}\sqrt{1-z^2}\cos\phi \equiv -\frac{N_T}{2}w. \tag{2.10}$$

The equations of motion (2.7) can be written in Hamiltonian form

$$\dot{z} = -\frac{\partial H}{\partial \phi}\ ;\ \dot{\phi} = \frac{\partial H}{\partial z}, \tag{2.11}$$

with

$$H = \frac{\Lambda z^2}{2} + \Delta E z - \sqrt{1-z^2}\cos\phi. \tag{2.12}$$

We now consider the SJJ tunneling equations, for comparison with the BEC tunneling equations above. The Josephson (charged) current of Cooper pairs $N_{1,2}$, with critical junction current $I_J \equiv 2eE_J/\hbar$, is given by

$$I = -2e(\dot{N}_1 - \dot{N}_2) \equiv I_J \sin\phi, \tag{2.13a}$$

and the Josephson frequency relation is

$$\hbar\dot{\phi} = \Delta\mu = 2ev_{ext} + E_c(N_1 - N_2), \tag{2.13b}$$

where ϕ is the superconductor phase difference, $\Delta\mu$ is the chemical potential difference, and v_{ext} is an applied voltage across the junction. $E_c(N_1 - N_2)$ is the capacitive charging energy induced by a Cooper pair imbalance $N_1 - N_2$, with $E_c = (2e)^2/2C$ the energy related to the transfer of a single pair, C being the junction capacitance. In terms of the fractional pair imbalance $z = (N_1 - N_2)/(N_1 + N_2)$, with $tE_J/N_T\hbar \to t$, Eqs. (2.13) become

$$\dot{z} = -\sin\phi \ ; \ \dot{\phi} = \Delta E_{SJJ} + \Lambda_{SJJ} z, \tag{2.14}$$

where now

$$\Delta E \equiv 2ev_{ext}N_T/E_J \ , \ \Lambda_{SJJ} \equiv E_c N_T^2/E_J. \tag{2.15}$$

For the SJJ, the requirement [7] that the chemical potential difference $\Delta\mu$ be smaller than the quasiparticle gap $2\Delta_{qp}$ (so as to prevent a jump onto the resistive $I - V$ branch), implies (for $v_{ext} = 0$) that $|z| < 2\Delta_{qp}/E_c N_T \sim 10^{-12}$, for typical parameters. The smallness of the upper bound is partly due to the fact that it involves a surface-to-bulk demension ratio. Very small fractional population imbalances of the charged pairs are sufficient to induce measurable voltages.

Comparing Eq. (2.14) with Eq. (2.7), we see that the SJJ equations are formally the linearized (in z) versions of the BEC equations. However, the macroscopic occupation of a single quantum state in the Bose case leads to a current scale $\sim \mathcal{K}\sqrt{N_T}$ Eq. (2.9) rather than the SJJ scale $\sim I_J$ of Eq. (2.13a). Thus we would expect analogs of the SJJ effects to occur in BEC, with important modifications due to nonlinearities in z, and possibly nonlinear effects not seen in SJJ. For the SJJ with external circuits one would monitor currents $\dot{z}$ and voltages $\dot{\phi}$. For the BEC, population imbalances $z(t)$ could be detected; there is no external circuit. However, external current drives can be imposed. $\dot{z}$ oscillations might be monitored by Doppler interferometric methods; there have been some attempts [18] to inject/extract atoms from traps in a controlled manner.

Mechanical analogs have been useful in visualizing the well-known Josephson effects of SJJ. The Hamiltonian governing Eq. (2.14) is

$$H = \Lambda_{SJJ} z^2/2 + \Delta E_{SJJ} z - \cos\phi, \tag{2.16}$$

and can be regarded (for $\Delta E_{SJJ} = 0$) as a 'particle' of mass Λ_{SJJ}^{-1}, 'linear momentum' $z \to p_x$ and spatial coordinate $\phi \to x$, moving on a rippled, rigid potential energy surface - $\cos\phi$. Alternatively, Eq. (2.16) describes a rigid pendulum of tilt-angle ϕ, moment of inertia Λ_{SJJ}^{-1}, angular momentum $z \to p_\phi$, and external forcing angular velocity $\sim \Delta E_{SJJ}$. The x and y linear pendulum-bob coordinates have a physical significance, as the SJJ tunneling currrent i and coupling energy e respectively, similar to Eqs. (2.9,2.10), with $x(t) = -\sin\phi \equiv i(t), y(t) = -\cos\phi \equiv w(t)$ and a rigid pendulum,

$$x^2 + y^2 = i^2 + w^2 = 1. \tag{2.17}$$

The Josephson effects in SJJ follow at once from physical considerations:

i. *Plasma oscillations*: For $\Delta E = 0$, the 'particle' of coordinate $x \leftrightarrow \phi$ can oscillate with small amplitude in one of the potential wells of $\cos\phi$. This corresponds to small, harmonic oscillations in angle ϕ of the rigid pendulum. Linearizing Eq. (2.14) in $\phi \ll 1$ yields $\ddot{z} \approx -\Lambda_{SJJ} z$ or a sinusoidal population imbalance oscillation,

$$z(t) \approx z(0)\cos\omega t - (\phi(0)/\omega)\sin\omega t, \tag{2.18}$$

where (in unscaled units),

$$\omega \approx \omega_p \equiv 2\pi/\tau_p = \Lambda_{SJJ}^{1/2} E_J/\hbar N_T = \sqrt{E_c E_J}/\hbar, \tag{2.19}$$

independent of initial conditions $z(0), \phi(0)$.

ii. *ac effect*: For a dc voltage $\Delta E \neq 0$, the particle has an imposed velocity, and moves between the $\cos\phi$ minima over the barriers. In the pendulum analogy, the external drive enforces rotatory motion at an angular velocity $\sim \Delta E_{SJJ}$. The phase, for $\Delta E \gg \Lambda|z|$ increases linearly with time, $\phi(t) \sim \Delta E t/\hbar$, and the sinusoidal $z(t)$ oscillation, similar to Eq. (2.18) has angular frequency

$$\omega = \omega_{ac} = \frac{2\pi}{\tau_{ac}} = \frac{\Delta E}{\hbar}, \tag{2.20}$$

independent of $z(0), \phi(0)$, and Λ.

iii. *Shapiro resonance effect*: If we have a small incremental ac voltage in addition to an applied dc voltage, $\Delta E \to \Delta E(1 + \delta_0 \cos\omega_0 t)$; $\delta_0 \ll 1$, then at resonance $\omega_0 = \omega_{ac}$, there is a dc tunneling current or a nonzero time average $\langle \dot{z}(t) \rangle \sim \delta_0 \langle \sin(\omega_{ac} t + \phi(0)) \sin\omega_0 t \rangle \neq 0$. This Shapiro resonance repeats at higher harmonics $\omega_{ac} = 2\pi/\tau_{ac} = n\omega_0, n = 1, 2, \ldots$, with characteristic Bessel function coefficients $J_n(n\delta_0)$ [7].

We expect that the BEC will show the analogs of these Josephson effects, with sinusoidal time dependences, in the limit $\Lambda \ll 1$, pr for general Λ, with $|z|, |\phi| \ll 1$. As shown numerically [14], for $\Lambda \lesssim 1$ and arbitrary z, the terms of Eq. (2.7) that are nonlinear in z lead to non-sinusoidal behaviour - these are *generalizations* of the SJJ effects. We will show that exact solutions for $z(t)$ are possible in terms of elliptic functions. The relevant signatures then appear as characteristic parameter dependences of the elliptic function *periods* similar to the Josephson oscillations of Eqs. (2.19, 2.20), but with strong deviations from the SJJ sinusoidal case.

The double-well BEC is a neutral superfluid system, like superfluid HeII. In the latter case, material tunneling barriers cannot exist. The only Josephson analog suggested has been [19] an imbalance in HeII heights $\langle h(t) \rangle$ between two baths connected by a submicron orifice, where vortex phase slips [20] occur at a steady rate. By the Josephson frequency relation, $\langle \dot{\phi}(t) \rangle = mg\langle h(t) \rangle$ this implies a gravitational chemical potential difference. As pointed out earlier [14], from From Eqs. (2.8),(2.15), however, the ability to tailor traps and the condensate self-interaction compensates for electrical neutrality, making the BEC double-well system more like a (charged) SJJ [7] than like HeII. Asymmetric positioning of the laser barrier could produce an energy difference ΔE, analogous to an applied voltage, since the effective potential seen by the atoms on the smaller-volume side will have a larger curvature and have a larger zero-point energy E^0. The (bulk) nonlinear atomic self-interaction $\sim UN_T z$ is like a (junction) capacitive charging energy $\sim E_c N_T z$.

The signatures for the generalized 'plasma' oscillation and 'ac' effect for the BEC, will appear in the period τ of the anharmonic oscillation as generalizations of Josephson frequencies of Eqs. (2.18),(2.20). In unscaled units, the inverse periods are:

$$\tau_p^{-1} = \sqrt{2UN_T\mathcal{K} + (2\mathcal{K})^2}/2\pi\hbar \;\; ; \;\; \tau_{ac}^{-1} = 2\mathcal{K}\sqrt{(\Delta E)^2 + 1}/2\pi\hbar. \tag{2.21}$$

Since the coupling energy $\mathcal{K} \sim A$, the tunnel junction area and UN_T the bulk interaction is independent of A, and the oscillation rate goes as $\tau_p^{-1} \sim A^{1/2}$. This can be checked by varying the intensity profile of the barrier laser beam, with a low-intensity to permit tunneling, only over a cross-section A. (The plasma frequency for SJJ, $\tau_p^{-1} \sim \sqrt{E_c E_J}$ by contrast, is independent of A, as $E_J \sim A, E_c \sim A^{-1}$.) The Josephson-like length '$\lambda_J' \equiv \sqrt{\hbar^2/2m\mathcal{K}}$, that governs spatial variation along the junction, should be much greater than $\sim \sqrt{A}$ to justify neglect of spatial variations of z, ϕ, i.e., obtain a 'flat plasmon' spectrum. For $\mathcal{K} = 0.1nK$, one finds '$\lambda_J' \sim 10\mu m$. We will not, however, consider such spatial variations here.

The nonlinearity in z, and parameter values of the BEC, supports other interesting behavior. Consider the $\Delta E = 0$ case. If the initial 'angular kinetic energy' of the pendulum (or 'linear kinetic energy' in the particle analogy), $z^2(0)$ exceeds a certain critical value, namely the potential energy barrier height — $\cos(\phi = \pi) = -1$ — of the vertically displaced $\phi = \pi$ 'pendulum orientation', there will occur a steady self-sustained 'pendulum rotation' (running particle motion). For BEC, one has Eq. (2.12), in contrast to Eq. (2.16). Rather than a unit-length pendulum, one has a *non*-rigid pendulum, with length

$$(x^2 + y^2)^{1/2} = (i^2 + w^2)^{1/2} = \sqrt{1 - z^2} \tag{2.22}$$

decreasing with 'angular momentum' z. The condition for the pendulum bob to roll over the 'vertical', is that the initial energy $H_0 \equiv H(z(0), \phi(0)) > -cos(\phi = \pi) = 1$. This implies novel behavior for $z(0), \phi(0), \Lambda$, satisfying

$$\Lambda > \frac{1 + \sqrt{1 - z^2(0)}\cos\phi(0)}{z^2(0)/2} \equiv \Lambda_c(z(0), \phi(0)). \tag{2.23}$$

Below the critical value Λ_c, the population imbalance oscillates about a zero value. Above Λ_c, the time-averaged 'angular momentum' is nonzero ($\langle z(t) \rangle \neq 0$), with oscillations around this nonzero value. The BEC maintains a nonzero dc population imbalance arising from the nonlinear self-interaction $\sim UN_T z^2$ of the atoms: the macroscopic imbalance is self-trapped. This may be termed 'macroscopic quantum self-trapping' (MQST). It differs from the He II imbalance [21], that arises from *external* gravitational effects. (For the BEC, gravitational effects merely result in a gravitational sag or shift of the 'centre of mass' of the wavefunction, as noted in Appendix A and in Ref. [22].) MQST also differs from the self-trapping of polarons [15] that arise from single electrons interacting with a polarizable lattice: it arises, instead, from self-interaction of a *macroscopically large*, coherent number of atoms.

The parameters UN_T, K, and E^0 can be estimated [14] to be $\sim 100nK, \sim 0.1nK$, and $\sim 10nK$ respectively for $N_T = 10^4$ if we take the trap-frequency ω_{trap} to be $\sim 100Hz$. Typical frequencies are then $1/\tau_p \sim kHz$, and $1/\tau_{ac} \sim kHz$ per nK energy difference, ΔE. The parameter Λ can be made to be of order unity, for $N_T \sim 10^6$ by changing the trap-frequency. Thus, with collective mode excitation energies $\Delta_{coll} \sim E^0$, and quasiparticle gaps $\Delta_{qp} \sim \sqrt{UN_T E^0}$ (as in Appendix A) the condition that excitations not be induced, allows for $|z| \lesssim O(1)$, i.e., even large population imbalances of the (neutral or un-excited) double-well BEC.

In the following Sections, we present exact solutions of Eq. (2.7) that yield experimentally verifiable predictions of phase-coherent signatures of BEC in double-well traps.

III. JOSEPHSON ANALOGS AND MQST: SYMMETRIC WELL CASE, $\Delta E = 0$

A. Exact solutions in terms of Jacobian elliptic functions

From the non-rigid pendulum analogy, the energy of the system is given by

$$H(z(t),\phi(t)) = \frac{\Lambda z^2}{2} + \Delta E z - \sqrt{1-z^2}\cos\phi = H(z(0),\phi(0)) \equiv H_0, \tag{3.1}$$

where H_0 is the initial (and conserved) energy. Using Eqs. (2.7a),(2.9),(2.22), the square of the pendulum length can be written as

$$\dot{z}^2 + (\sqrt{1-z^2}\cos\phi)^2 = 1 - z^2. \tag{3.2}$$

Combining Eqs. (3.1) and (3.2) we have

$$\dot{z}^2 + \left[\frac{\Lambda z^2}{2} + \Delta E z - H_0\right]^2 = 1 - z^2. \tag{3.3}$$

As in polaronic contexts [15,23–26] we use Eq. (3.3) to obtain the exact solution for $z(t)$ in terms of quadratures,

$$\frac{\Lambda t}{2} = \int_{z(t)}^{z(0)} \frac{dz}{\sqrt{\left(\frac{2}{\Lambda}\right)^2 (1-z^2) - \left[z^2 + \frac{2z\Delta E}{\Lambda} - \frac{2H_0}{\Lambda}\right]^2}} \tag{3.4}$$

We consider $\Delta E = 0$, and $\Delta E \neq 0$ cases separately. The first draws directly on previous results by Kenkre and collaborators [15,23,26–28], and work related to the second is to be found in Ref. [29]. For symmetric double wells, $\Delta E = 0$, Eq. (3.4) becomes

$$\frac{\Lambda t}{2} = \int_{z(t)}^{z(0)} \frac{dz}{\sqrt{(\alpha^2 + z^2)(C^2 - z^2)}}, \tag{3.5}$$

where

$$C^2 = \frac{2}{\Lambda^2}\left[(H_0\Lambda - 1) + \frac{\zeta^2}{2}\right] \; ; \; \alpha^2 = \frac{2}{\Lambda^2}\left[\zeta^2 - (H_0\Lambda - 1)\right], \tag{3.6a}$$

$$\zeta^2(\Lambda) = 2\sqrt{\Lambda^2 + 1 - 2H_0\Lambda}. \tag{3.6b}$$

The solution to Eq. (3.5) is known in general (see, e.g., Refs. [15,23]) and is written as

$$z(t) = C\mathrm{cn}[(C\Lambda/k)(t-t_0), k] \text{ for } 0 < k < 1$$
$$= C\mathrm{dn}[(C\Lambda)(t-t_0), 1/k], \text{ for } k > 1; \tag{3.7a}$$
$$k^2 = \frac{1}{2}\left(\frac{C\Lambda}{\zeta(\Lambda)}\right)^2 = \frac{1}{2}\left[1 + \frac{(H_0\Lambda - 1)}{\sqrt{\Lambda^2 + 1 - 2H_0\Lambda}}\right], \tag{3.7b}$$

where t_0 is a constant determined from the initial population imbalance, $z(0)$ and initial energy H_0 (see Appendix B), and the functions cn and dn are the Jacobian elliptic functions with k the elliptic modulus. In Appendix B, we provide, for completeness, some definitions and properties of elliptic functions. The character of the solution changes when elliptic modulus $k = 1$. From Eqs. (2.23),(3.7b), this mathematical condition (2.23) corresponds to the physical condition $H_0 = 1, \Lambda = \Lambda_c$, for the onset of MQST. The evolution of the imbalance is given, in this special case, by the non-oscillatory hyperbolic function

$$z(t) = C\mathrm{cn}[(C\Lambda_c)(t-t_0), 1] = C\mathrm{sech}C\Lambda_c(t-t_0)\ ,\ C = \frac{2\sqrt{\Lambda_c - 1}}{\Lambda_c} \tag{3.7c}$$

The Jacobian elliptic functions $\mathrm{cn}(u,k)$ and $\mathrm{dn}(u,k)$ are periodic in the argument u with period $4K(k)$ and $2K(k)$ respectively where $K(k)$ is the complete elliptic integral of the first kind (Appendix B). Thus, the time-period of oscillation of $z(t)$ is given by [30]

$$\tau = \frac{4kK(k)}{C\Lambda} \text{ for } 0 < k < 1, \tag{3.8a}$$
$$= \frac{2K(1/k)}{C\Lambda} \text{ for } k > 1. \tag{3.8b}$$

The period is infinite, as in critical slowing down, diverging logarithmically, $K(k) \to ln(4/\sqrt{1-k^2})$ as $k \to 1$, or $\Lambda \to \Lambda_c$. diverging logarithmically, as noted in Appendix B.

The elliptic functions in Eqs. (3.7) can be expanded in a Fourier series [30]. As the non-linear parameter $\Lambda \to 0$, i.e., $k \to\sim \Lambda$, single harmonic sinusoidal dependences are recovered, as in the SJJ case. Using Eqs. (3.7), the time-fourier transform, $z(\omega) \equiv (1/2\pi)\int_0^{2\pi} dt e^{i\omega t} z(t)$ can, therefore, be written exactly as,

$$z(\omega) = \frac{z(0)}{4kK(k)} \sum_{n=0}^{\infty} \mathrm{sech}\left[\frac{(n+1/2)\pi K'(k)}{K(k)}\right][\delta(\omega \pm \omega_n^<)] \text{ for } 0 < k^2 < 1, \tag{3.9a}$$
$$= \left(\frac{1}{2\Lambda}\right)\mathrm{sech}(\omega/\omega_c) \text{ for } k^2 = 1, \tag{3.9b}$$
$$= \frac{z(0)}{4K(1/k)}\left(\delta(\omega) + \sum_{n=1}^{\infty} \mathrm{sech}\left[\frac{n\pi K'(1/k)}{K(1/k)}\right][\delta(\omega \pm \omega_n^>)]\right] \text{ for } k^2 > 1, \tag{3.9c}$$
$$= \frac{z(0)}{4k_1K'(k_1)}\left(\delta(\omega) + \sum_{n=1}^{\infty}(-1)^n \mathrm{sech}\left[\frac{n\pi K'(k_1)}{K(k_1)}\right][\delta(\omega \pm \Omega_n)]\right] \text{ for } k^2 < 0, \tag{3.9d}$$

where

$$\omega_n^< = \frac{(n+1/2)\pi z(0)\Lambda}{kK(k)} \ , \ \omega_n^> = \frac{n\pi z(0)\Lambda}{K(1/k)} \ , \ \Omega_n = \frac{n\pi z(0) 2\Lambda}{k_1 K(k_1)} \tag{3.10a}$$

$$\omega_c = \frac{2z(0)\Lambda_c}{\pi} \ , \ k_1 = \frac{|k|}{\sqrt{1+|k|^2}} \ , \ K'(k) \equiv K(\sqrt{1-k^2}). \tag{3.10b}$$

In the expressions above Eqs. (3.9), we have assumed initial conditions such that $\phi(0) = 0, \pi$ for simplicity. Choice of other initial values of ϕ merely adds an irrelevant phase to the fourier components with no shift in the frequencies themselves: the qualitative behavior is independent of the initial phase $\phi(0)$, that is harder to fix than the initial imbalance $z(0)$.

B. Discussion of results

As Eq. (3.4) shows, the dynamics is governed by two initial values $z(0), H_0$. However, we note that $z(0), \phi(0)$ are equally valid initial parameter values and work with them for the remainder of the paper. In particular, from Eq. (3.1) note that the two extreme initial conditions $\phi(0) = 0, \pi$ correspond to the two extreme values of H_0 (for a fixed value of $z(0)$), $H_0 = \frac{\Lambda z(0)^2}{2} \pm \sqrt{1-z(0)^2}$. Equations (3.7),(3.8),(3.9) constitute predictions for measurements of population imbalances $z(t)$, the period τ, and the frequency spectrum $z(\omega)$, in terms of tabulated elliptic functions [30,31].

In the figures, we consider $U > 0, \Lambda > 0$, for $\phi(0) = 0, \pi$. The case $U < 0, \Lambda > 0$ corresponds to a negative scattering length, as may occur for lithium atoms, where the condensate may be stable only for low densities [22]. The dynamical equation (3.5) is invariant under the transformation $\Lambda \to -\Lambda, \phi(0) \to \pi - \phi(0)$ ($H_0 \to -H_0$ in that case from Eq. (3.1)). Thus the special case $\phi(0) = \pi$ with $\Lambda > 0$ that we shown in the figures, may physically correspond to the behavior of $\Lambda < 0$ atoms with $\phi(0) = 0$. We remark that the general behavior of the time-period, of Λ_c, as well as the Fourier spectrum for arbitrary values of $0 \leq \phi(0) < \pi$ are similar to those corresponding to $\phi(0) = 0$. The $\phi(0) = \pi$ case is also considered for its special properties and because it may correspond, as discussed earlier, to negative scattering length atoms with $\phi(0) = 0$. In all the figures, the $\phi(0) = 0, \pi$ cases are shown as dotted and dashed lines respectively, unless otherwise mentioned.

Figures 2(a)-(d) show the predicted $z(t)$ oscillations from Eqs. (3.7a), with $z(0) = 0.6, \phi(0) = 0$ and various values of Λ as shown. These match previous [14] numerical solutions. For $\Lambda = 1$, Fig. 2(a), we have almost pure sinusoidal 'plasma' oscillations around

a zero time-average $\langle z \rangle = 0$. [16,32,33] (Rabi oscillations of frequency $2\mathcal{K}$, correspond to the unphysical limit $\Lambda = U = 0$ of the *non*-interacting, ideal Bose gas.) *Non*-sinusoidal oscillations are more typical – these are *generalized* Josephson 'plasma' oscillations, shown in Fig. 2(b)-(d). At $\Lambda = \Lambda_c$ (10 in this case), the timeperiod of oscillations diverges, $\tau = \infty$, signaling the onset of MQST, and the nonoscillatory Eq. (3.7c) yields the dashed line in Fig. 2d.

Figures 3(a)-(d) show, for various $z(0)$, the reciprocal of the timeperiod, $1/\tau$, given by Eq. (3.8), expressed in dimensionless form by being scaled by $1/\tau_p$ of Eq. (2.21), as a function of Λ/Λ_c. The period of the non-sinusoidal $z(t)$ of Fig. 2 shifts from the simple SJJ-type value of unity, attained only in the $\Lambda \sim U \to 0$ ideal Bose gas limit. Note that $\tau_p \sim 1/\sqrt{\Lambda + 1}$ decreases with Λ. For $\phi(0) = 0$, the unscaled $1/\tau$ actually rises with Λ before falling as MQST sets in at $\Lambda = \Lambda_c$ signified by the dip $1/\tau \to 0$. This corresponds to the dashed-line $z(t)$ time-evolution in Fig. 2(d). For $\Lambda/\Lambda_c > 1$, there is a non-zero time-average ($\langle z(t) \rangle \neq 0$) value (inset of Fig. 3(a)) and τ_p/τ above the dip describes the time period of oscillations around this. The sensitivity of the curves to initial $\phi(0)$ values decreases as the initial population imbalance increases, and for the (unphysical) value of $z(0) = 1$, the $\phi(0) = 0, \pi$ curves merge, as in Fig. 3(d). Whereas for the case when $\phi(0) = 0$, the MQST dip is abrupt,for $\phi(0) = \pi$, the transition dip is much more gradual. This observation will be elaborated later in this Section. In both cases, however, the divergence of the time-period τ is logarithmic [23] (see Appendix B). Note that from Eq. (2.23), Λ_c increases as $1/z^2(0)$ for $z(0) \to 0$, for the range $0 \leq \phi(0) < \pi$, while $\phi(0) = \pi$ is special case, $\Lambda_c \to 1$ as $z(0) \to 0$. For $\phi(0) = 0, \Lambda_c \sim 400$, while for $\phi(0) = \pi, \Lambda_c \sim 1$.

As noted earlier, $\phi(0) = 0, \Lambda < 0$ corresponds to $\phi(0) = \pi, \Lambda > 0$. For $\phi(0) = \pi, \Lambda > \Lambda_c > 0$, for a special value, $\Lambda = -\frac{\cos\phi(0)}{\sqrt{1-z_0^2}}$, ζ of Eq. (3.6b) can become zero and k^2 can become infinite. The system is then placed in a *self-trapped stationary state* [27], $z(t) = z(0)$ for all time. An increase of Λ beyond this value (in magnitude) results in an intriguing situation: the condensates transfer more of their population into the initially populated trap, i.e., the time-averaged value $\langle z(t) \rangle > z(0)$. The atomic flow is 'uphill', settling to a higher dc imbalance than initially. This feature is illustrated clearly in the inset of Fig. 3(a). $z(0) = 0.1$ and with the solid (dashed) line referring to the initial condition $\phi(0) = 0(\pi)$. When $\phi(0) = 0$, the time-averaged value of the imbalance $\langle z \rangle$ always remains less than the initial value $z(0)$ and approaches this value from below for large values of Λ/Λ_c. On the contrary, when $\phi(0) = \pi$ (dashed line), the average value rapidly increases to ~ 0.45, i.e.,

larger than the initial value $z(0) = 0.1$, decreasing to 0.1 from above, for large Λ/Λ_c. The initial phases can induce a flow from the less populated to the more populated trap. This is in keeping with the observation of the 'amplitude transition' in Refs. [26,27].

In Fig. 4, the Fourier spectrum $z(\omega)$ of Eq. (3.9) is displayed. Figures 4 (a)-(f) show the normalized spectrum $z(\omega)/z(\omega)_{max}$ as a function of the scaled frequency ω/Λ. ($z(\omega)_{max}$ is defined as the strength of the largest peak in $z(\omega)$; values are as stated in the figures. As a function of Λ/Λ_c, $z(\omega)_{max}$ remains finite with a sharp dip to a value $1/\Lambda_c$ at $\Lambda = \Lambda_c$.) Here, $z(0) = 0.1$ in all the figures and the ratio Λ/Λ_c is increased from 0.1 to 1.01 in (a)-(d). For small values of Λ/Λ_c, Fig. 4(a), only the $\phi(0) = 0$ dotted lines are visible since the $\phi(0) = \pi$ dashed lines are outside the region shown. The separation between positive/negative frequency peaks is reduced for larger values of Λ/Λ_c and more lines appear. At the onset of MQST, there is an explosion of frequencies and all the lines merge into a band at $\Lambda/\Lambda_c = 1$, that is the same $\phi(0) = 0, \pi$. For $\Lambda > \Lambda_c$, there is a remnant delta-function peak at zero-frequency representing that $\langle z(t) \rangle \neq 0$, with side frequencies that march outward as Λ is increased. Note that despite the fact that both the curves collapse onto the same curve at $\Lambda/\Lambda_c = 1$, in actual magnitude, the width of the spectrum at the transition for the $\phi(0) = \pi$ is much less compared to the $\phi(0) = 0$ case, since Λ_c values differ widely. We remark that although we analyze only two special cases $\phi(0) = 0, \pi$, the general behaviour of the time-period as well as the Fourier spectrum for arbitrary values of $\phi(0)$ are similar to those corresponding to $\phi(0) = 0$.

IV. JOSEPHSON ANALOGS AND MQST: ASYMMETRIC TRAP CASE, $\Delta E \neq 0$

A. Exact solutions in terms of Weierstrassian elliptic functions

Let us now analyze the case where the traps are asymmetric, i.e., $\Delta E \neq 0$, as in Fig. 1, and return to Eq. (3.4),

$$\frac{\Lambda t}{2} = \int_{z(t)}^{z(0)} \frac{dz}{\sqrt{f(z)}}, \tag{4.1a}$$

$$f(z) = \left(\frac{2}{\Lambda}\right)^2 (1 - z^2) - \left[z^2 + \frac{2z\Delta E}{\Lambda} - \frac{2H_0}{\Lambda}\right]^2 \tag{4.1b}$$

As outlined in Appendix B, the solution to Eq. (4.1) for the fractional population imbalance $z(t)$ is given as

$$z(t) = z_1 + \frac{6f'(z_1)}{24\wp(\Lambda(t-t_0)/2; g_2, g_3) - f''(z_1)}, \tag{4.2a}$$

$$g_2 = -a_4 - 4a_1a_3 + 3a_2^2 \; ; \; g_3 = -a_2a_4 + 2a_1a_2a_3 - a_2^3 + a_3^2 - a_1^2a_4, \tag{4.2b}$$

$$a_1 = -\frac{\Delta E}{\Lambda} \; ; \; a_2 = \frac{2}{3\Lambda^2}(\Lambda(H_0+1) - \Delta E^2) \; ; \; a_3 = \frac{2H_0\Delta E}{\Lambda^2} \; ; \; a_4 = \frac{4(1-H_0^2)}{\Lambda^2}, \tag{4.2c}$$

where $\wp(t; g_2, g_3)$ is the Weierstrassian elliptic function, t_0 is a constant determined from the initial conditions $z(0), H_0$, and z_1 is a real root of $f(z)$. In terms of the non-rigid pendulum analogy, z_1 corresponds to that point of the evolution where the instantaneous angular velocity vanishes, $\dot{z}|_{z=z_1} = 0$, or from Eq. (3.3) when $\phi = 0, \pi$. The fractional population difference $z(t)$ in Eq. (4.2) can also be written in terms of Jacobian elliptic functions by making use of the usual relations between the elliptic functions [34]. The key quantity governing the behaviour of the Weierstrassian elliptic function is the discriminant, defined as $\delta = g_2^3 - 27g_3^2$. The relationships between these functions depending on the sign of δ are detailed in Ref. [24] and reviewed in Appendix B. These results go beyond the $\Delta E = 0$ solutions found in Refs. [15,23] and are equivalent to those of Ref. [29] for a similar polaronic system and those of Refs. [24,25] in different contexts.

A closed form evaluation of the spectrum was given for the symmetric trap, $\Delta E = 0$. This is not possible for the asymmetric case, $\Delta E \neq 0$. However, it is still possible to calculate analytically the time-period of the solutions in Eqs. (B19,B21a, B22,B23,B24) in terms of the complete elliptic integral of the first kind [34]. Since we will be discussing the properties of the time-period of oscillation later in this Section, we give below a brief listing of the explicit dependence of the time-period τ on the parameters of the problem,

$$\tau = K(k_1)/(e_1 - e_3), \text{ for } \delta > 0, \tag{4.3a}$$

$$\tau = K(k_2)/\sqrt{H_2}, \text{for } \delta < 0, \tag{4.3b}$$

$$\tau = \infty, \text{for } \delta = 0, g_2 > 0, g_3 < 0, \tag{4.3c}$$

$$\tau = \pi/\sqrt{6g_3^{1/3}}, \text{for } \delta = 0, g_2 > 0, g_3 > 0, \tag{4.3d}$$

$$\tau = \infty, \text{for } \delta = 0, g_2 = g_3 = 0, \tag{4.3e}$$

where $K(k)$ is the complete elliptic integral of the first kind and $k_{1,2}, e_{1,2,3}, g_{2,3}$ are defined in Eqs. (4.2b, B22,B23,B24).

B. Discussion of results

Figure 5 shows the scaled reciprocal of the period τ_{ac}/τ plotted as a function of the scaled nonlinearity ratio $\Lambda/\Lambda_c(\Delta E)$ where τ_{ac} is defined in Eq. (2.21) and $\Lambda_c(\Delta E)$ denotes the value of Λ at which $\tau \to \infty$. This is like Fig. 3. Here, $z(0) = 0.1, \Delta E = 1.0$. Insets (a) and (b) show the time-averaged value, $\langle z(t) \rangle$ plotted as a function of Λ/Λ_c for $\phi(0)$ and $\phi(0) = \pi$ respectively. The results are similar to those in Fig. (3), with a dip at the onset of MQST, but now with a skew due to the trap asymmetry ΔE. Note that the dip now denotes the separation of *two* kinds of trapping or localization of the condensate, where $\langle z \rangle \neq 0$, now on both sides, as in the insets. For $\Lambda < \Lambda_c(\Delta E)$, the condensate is localized, $\langle z \rangle \neq 0$, entirely due to the 'disorder' or trap asymmetry. (For $\Delta E = 0$, this regime is marked by $\langle z \rangle = 0$.) At $\Lambda = \Lambda_c$ itself, the system is on the phase-boundary: $\tau \to \infty, \langle z \rangle = 0$. When $\Lambda > \Lambda_c$, the condensate is again localized or self-trapped, and again $\langle z \rangle \neq 0$, but this time it is due to the self-interaction, in a $\Delta E \neq 0$ version of MQST.

There are a few key differences between these two kinds of localization as the insets (a) and (b) show. Let us look at the $\phi(0) = 0$ inset (a) first. When $\Lambda < \Lambda_c$, $\langle z \rangle > 0$ and is governed by the combined influence of $z(0), \phi(0), \Delta E$. Furthermore, the absolute value can be much larger than $z(0)$. This fact is reinforced in inset (b) also. On the contrary, note that for large values of Λ (with MQST trapping), the actual value of $\langle z(t) \rangle$ approaches the initial imbalance value $z(0)$ and is independent of $\phi(0)$. Thus, whereas the nonlinear self-interaction does act as an effective 'disorder' [26,27], there do exist significant differences between the two kinds of localization.

Figures 6 (a,b) show, for $\phi(0) = 0, \pi$ respectively, the scaled reciprocal of the period τ_{ac}/τ as a function of the trap asymmetry ΔE for different values of Λ/Λ_c, where τ_{ac} is as defined in Eq. (2.21). Note that, unlike Fig. 5, Λ_c is now the critical value of Λ at which MQST sets in, in the *absence* of trap asymmetry, $\Delta E = 0$. The simple ac Josephson effect value $\tau_{ac}/\tau = 1$ is approached for all curves, for large positive and negative values of ΔE (when trap asymmetry effects dominate nonlinear effects). The MQST dip in τ_{ac}/τ shows up (for fixed Λ/Λ_c close to unity) as ΔE passes through critical values.

V. SHAPIRO EFFECT ANALOGS

Let us now consider the analog of the Shapiro resonance effect observed in SJJ [7]. In addition to a time-independent trap asymmetry ΔE, we impose a sinusoidal variation so that we can write the asymmetry term as $\Delta E + \Delta_1 \cos\omega_0 t)$. This could be done by varying the laser barrier position at fixed intensity. A similar Shapiro-like resonance effect could be seen, with an oscillation of the laser beam intensity, at fixed mid-position, so $\mathcal{K} \to \mathcal{K}(1 + \delta_0 \cos\omega_0 t)$. The analog of the Shapiro effect arises when the period from the time independent asymmetry, $\sim 1/\Delta E$, matches that from the oscillatory increment, $\sim 1/\omega_0$. This matching condition is intimately connected with the phenomenon of Bloch oscillations and dynamic localization in crystals [35–38] and trapping in two-level atoms [39]. We analyze the dc value of the drift current, $\langle \dot{z}(t) \rangle$, and plot it as a function of ΔE, where resonances shown up as spikes. (For SJJ, with current drives, the Shapiro effect shows up as steps in the I-V characteristics.) Of course, the dc drift cannot persist indefinitely, as when the population in one well drops below N_{min}, phase difference will collapse.

Figure 7 shows $I_{dc} \propto \langle \dot{z}(t) \rangle$ obtained from time averaging the numerical solution, with a small ac drive and $\Delta E \neq 0$. It is plotted as a function of $\Delta E/\omega_0$ for increasing values of the nonlinearity ratio Λ. The initial conditions are $z(0) \sim 0 = 0.045, \phi(0) = \pi/2$, for which $\Lambda_c \sim 1000$ (in the absence of ΔE and ac driving). When Λ is zero, the analog of the 'Shapiro effect' occurs, with sharp peaks in I_{dc} occurs whenever $\Delta E \propto n\omega_0, n = 1, 2, \ldots$. As Λ increases, however, two things happen. Firstly, multiple peaks also occur at $\Delta E/\omega_0$ values different from integers. Close to the MQST regime, ($\Lambda \sim \Lambda_c$), there is a proliferation of peaks as the system moves from a regime of constant current, $\langle \dot{z} \rangle \neq 0$ (Λ small), to one of constant population imbalance $\langle z \rangle \neq 0$ (Λ large). Secondly, the magnitude of the peaks or dc currents decreases.

VI. POSSIBLE EXPERIMENTAL PROCEDURES, AND SUMMARY

In order to illustrate experimental issues, we now discuss possible 'gedanken' procedures to set up initial conditions, determine parameters, and cast data in terms of theoretical plots.

i. *Fixing initial* $z(0), \phi(0)$: With no barriers, the phase of the BEC will be locked across the single well. A strong laser barrier will produce two BEC with a common phase,

$\phi(0)$. If the barrier is off-center, it captures $N_1 \neq N_2$ populations, $z(0) \neq 0, \Delta E \neq 0$. Moving the barrier to the center, so $\Delta E = 0$, sets up initial conditions for plasma oscillations to occur, when the barrier is lowered to permit tunneling. The zero initial current $\dot{z}(0) = 0$ is consistent with $\phi(0) = 0$. (Alternatively, the strong laser barrier could be switched on at mid-point, so $\Delta E = 0$, but $N_1 = N_2$; atoms could then be slowly added to one well, to set up the $z(0) \neq 0, \phi(0) = 0$ state.)

In the SJJ, external dc current drives $I_{ext} = I = I_0 \sin\phi$ force phases apart $\phi = \sin^{-1}(I_{ext}/I_{dc})$, with $\phi = \pi/2$ when the dc current rises to a maximum $I_{ext} = I_J$. Speculatively, if the magnetic trap profile along the outer edges could be reduced along a direction perpendicular to the laser sheet barrier, then a stream of atoms could be injected in one well an be ejected from the other well, tunneling through the intervening barrier, in a steady state, analogous to the dc Josephson effect. Switching off the dc 'current drive' would leave the BEC phase difference at nonzero values.

ii. *Experimental Sequence*: The theoretical predictions are in terms of the parameter $\Lambda = UN_T/2\mathcal{K}$, and scaling times are τ_p, τ_{ac}. Λ can be varied by changing the total density of atoms $\sim N_T$ with $U, \mathcal{K}$ also functions of density. Λ can also be varied by varying the coupling $\mathcal{K} = \mathcal{K}(\mathcal{I}, d)$ that depends on the intensity $\mathcal{I}$ and (exponentially) on the thickness d, of laser-sheet barrier. We suggest an experimental sequence based on variations of $\mathcal{I}, d$, with N_T constant, and present a plot more directly connected to measurable quantities.

Suppose we set up a $z(0) \ll 1, \phi(0) = 0, \Delta E = 0$ state and measure the oscillation period τ for a range of $\mathcal{K}(\mathcal{I}, d)$ corresponding to a range of $\Lambda = UN_T/2\mathcal{K}(\mathcal{I}, d)$. Then this measured τ, that we call τ^* say, will correspond to plasma oscillations, and serves as a calibration curve for different later experiments with different initial conditions. Now suppose we measure τ for other $z(0) \lesssim 1, \phi(0) = 0$ initial conditions, over the *same* range of control parameters, i.e., of Λ. If $\Lambda_c \sim 1/z^2(0)$ is within the range of Λ explored, MQST dips in $1/\tau$ will be seen at critical values of $\mathcal{I}$ or d. Now, we plot $1/\tau$ versus $1/\tau^*$ noting the $1/\tau_c^*$ values where the dips occur. A final scaled data plot of τ^*/τ versus τ_c^*/τ^* is suitable for theoretical comparison.

Figure 8(a) shows a theoretical plot of $2\pi\hbar/UN_T\tau$ versus Λ for illustrative values $z(0) = 0.02$ (dotted line), and $z(0) = 0.4, 0.6$ (solid lines), with $\phi(0) = 0$. (Here we scale in $UN_T/\hbar$, assumed fixed, instead of $\mathcal{K}$, as previous.) The dashed line, indicating

the plasma oscillation behavior that is now $1/\tau_p(\Lambda) = UN_T\sqrt{\Lambda^{-1}+\Lambda^{-2}}$ clearly closely follows the dotted line, $\tau(z(0)=0.02,\phi(0)=0,\Lambda)=\tau_p(\Lambda)$. The solid lines show MQST dips at different $\Lambda=\Lambda_c(z(0))$ values, corresponding to values $\tau_{pc}(z(0))$ of the dotted line.

Figure 8(b) shows the theoretical plot of τ_p/τ versus $\tau_{pc}/\tau_p = \sqrt{\Lambda^{-1}+\Lambda^{-2}}/\sqrt{\Lambda_c^{-1}+\Lambda_c^{-2}}$ that can be directly compared with experimental data of τ^*/τ versus τ_c^*/τ^*. The $\tau_p(\Lambda)$ calibration curve procedure can also be followed for the $\Delta E \neq 0$ case.

iii. *Data Collapse*: Figure 8(b) shows that the curves are different for different $z(0)$. Can we cast the theoretical curves/experimental data so that data collapse occurs to a universal form, common for all $z(0)$? From the above discussion, the bridge between theory and experiment is $\tau_c^*/\tau^* = \sqrt{\Lambda^{-1}+\Lambda^{-2}}/\sqrt{\Lambda_c^{-1}+\Lambda_c^{-2}}$. Thus, (for a given $z(0)$), $\Lambda = 2/(1+[1+(2\tau_c^*/\tau^*)^2\sqrt{\Lambda_c^{-1}+\Lambda_c^{-2}}]^{1/2})$. Now, from Eq. (3.8), the scaled period $C\Lambda/\tau$ can be expressed as a function of $k^2 = k^2(\Lambda, z(0), \phi(0))$ given by Eq. (3.7b). Thus we can cast the data in a universal curve of $C\Lambda/\tau$ versus k^2, common to all $z(0)$, that is all a complete elliptic integral of the first kind.

To summarize, we have presented analytic solutions in terms of elliptic functions for the population imbalance as a function of time and for the period of imbalance oscillations for a model describing Bose-Einstein condensate tunneling. The observation of predicted Josephson effect generalizations to non-sinusoidal oscillations both in time and frequency; and of a blocking of tunneling by self-trapping due to nonlinear self-interaction, and/or asymmetric traps constitute experimentally verifiable tests of quantum phase coherence in BEC.

APPENDIX A: DERIVATION OF GPE EQNS.

We sketch the derivation from the basic Hamiltonian describing a system of interacting bosons in an external potential leading to the GPE. In the treatment below, we shall follow closely earlier work [40,41,43]. Our starting point is the basic Hamiltonian

$$H = -\int d^3\mathrm{r}\hat{\psi}^\dagger(\mathrm{r})\frac{\hbar^2\nabla^2}{2m}\hat{\psi}(\mathrm{r}) + \int d^3\mathrm{r}V_{ext}(\mathrm{r})\hat{\psi}^\dagger(\mathrm{r})\hat{\psi}(\mathrm{r}) + \frac{1}{2}\int d^3\mathrm{r}\int d^3\mathrm{r}' U(\mathrm{r}-\mathrm{r}')\hat{\psi}^\dagger(\mathrm{r})\hat{\psi}^\dagger(\mathrm{r}')\hat{\psi}(\mathrm{r}')\hat{\psi}(\mathrm{r}), \quad \text{(A1)}$$

where the field operators $\hat{\psi}^\dagger(\mathbf{r}), \hat{\psi}(\mathbf{r})$ can be written in terms of the boson creation and destruction operators of an as yet unspecified single-particle basis $\{\phi_\alpha(\mathbf{r})\}$

$$\hat{\psi}(\mathbf{r}) = \sum_\alpha \hat{a}_\alpha \phi_\alpha(\mathbf{r}). \tag{A2}$$

Here, $U(\mathbf{r}-\mathbf{r}')$ is the interaction between the particles and $V_{ext}(\mathbf{r}) = \frac{1}{2}m\omega_{trap}^2\mathbf{r}^2 - mgz = \frac{1}{2}m\omega_{trap}^2(\mathbf{r}-\mathbf{r}_g)^2 - \frac{1}{2}\frac{mg}{\omega_{trap}^2}$ describes the external harmonic trap potential including effects of gravitational acceleration g, that enters as a 'sag' or shift of the wavefunction's postion, $\mathbf{r}_g = (0,0,\frac{g}{\omega_{trap}^2})$. We simplify the calculations by taking a contact interaction for the self-interacting term, $U(\mathbf{r}-\mathbf{r}') = g_0\delta(\mathbf{r}-\mathbf{r}')$. We thus arrive at the following equation of evolution for $\hat{\psi}(\mathbf{r})$,

$$i\hbar\frac{\partial\hat{\psi}(\mathbf{r})}{\partial t} = -\frac{\hbar^2}{2m}\nabla^2\hat{\psi}(\mathbf{r}) + V_{ext}\hat{\psi}(\mathbf{r}) + g_0\hat{\psi}^\dagger(\mathbf{r})\hat{\psi}(\mathbf{r})\hat{\psi}(\mathbf{r}). \tag{A3}$$

As sketched, for example in Refs. [40,41], by following Bogolyubov-type [42] procedures, we obtain mean-field equations for the boson eigenfunctions ϕ_α,

$$-\frac{\hbar^2}{2m}\nabla^2\phi_\alpha(\mathbf{r}) + 2(\rho_n(\mathbf{r}) + \rho_0(\mathbf{r}))g_0\phi_\alpha(\mathbf{r}) + v_{ext}\phi_\alpha(\mathbf{r}) = \epsilon_\alpha\phi_\alpha(\mathbf{r}), \qquad \alpha \neq 0 \tag{A4a}$$

$$-\frac{\hbar^2}{2m}\nabla^2\phi_0(\mathbf{r}) + 2\rho_n(\mathbf{r})g_0\phi_0(\mathbf{r}) + \rho_0(\mathbf{r})g_0\phi_0(\mathbf{r}) + v_{ext}\phi_0(\mathbf{r}) = \epsilon_0\phi_0(\mathbf{r}), \tag{A4b}$$

where

$$\rho_n(\mathbf{r}) = \sum_{\alpha\neq 0} n_\alpha|\phi_\alpha(\mathbf{r})|^2 \tag{A5}$$

is the density of the 'normal component' and $\rho_0(\mathbf{r}) = n_0|\phi_0(\mathbf{r})|^2$ is the condensate density, $n_\alpha = [\exp(\beta(\epsilon_\alpha - \mu)) - 1]^{-1}$ and $n_0 = [\exp(\beta(\epsilon_0 - \mu)) - 1]^{-1}$ are the occupation numbers, and μ is the chemical potential.

At zero temperature, we only consider the $\alpha = 0$ ground state component of Eqs. (A4) and obtain the GPE equation (2.1)

$$i\hbar\frac{d\Psi(r,t)}{dt} = -\frac{\hbar^2}{2m}\nabla^2\Psi(r,t) + [V_{ext}(r) + g_0|\Psi(r,t)|^2]\Psi(r,t), \tag{A6}$$

where $\Psi(r,t) = \phi_0(r)e^{-i\epsilon_0 t}$. One sees from Eq. (A4b) that the primary effect of finite temperature is to alter the energy ϵ_0, and hence, later, the zero-point energies $E_{1,2}^0$ in the double-well case. For BEC tunneling between two symmetric traps, this temperature dependence will

cancel. Thus our results of the symmetric trap case discussed for zero temperature are valid for finite temperature as well. However, for asymmetric traps, one has to consider finite temperature effects with more care.

As in Ref. [14], we now derive the basic tunneling equations Eqs. (2.4) from the GPE eigenvalue equation, Eqs. (2.2). We take a trial solution in the form

$$\Psi(r,t) = \psi_1(t)\Phi_1(r) + \psi_2(t)\Phi_2(r)\ ;\ \psi_{1,2} = \sqrt{N_{1,2}}(t)e^{i\theta_{1,2}(t)}, \tag{A7}$$

where $\Phi_{1,2}(r)$ are the time-independent GPE solutions for two independent traps, (2.2). With the restrictions

$$\int d^3r|\Phi_{1,2}(r)|^2 = 1\ ,\ \int d^3r\Phi_1(r)\Phi_2(r) \simeq 0, \tag{A8}$$

we define parameters,

$$E^0_{1,2} = \int d^3r\left[\frac{\hbar^2}{2m}|\nabla\Phi_{1,2}|^2 + V_{ext}(r)\Phi^2_{1,2}(r)\right], \tag{A9a}$$

$$U_{1,2} = g_0\int d^3r\Phi^4_{1,2}(r), \tag{A9b}$$

$$\mathcal{K} = -\int d^3r\left[\frac{\hbar^2}{2m}(\nabla\Phi_1(r)\cdot\nabla\Phi_2(r)) + V_{ext}(r)\Phi_1(r)\Phi_2(r)\right], \tag{A9c}$$

and obtain the following GPE equations for the amplitudes $\psi_{1,2}(t)$, (2.4),

$$i\hbar\frac{\partial\psi_1}{\partial t} = (E^0_1 + U_1N_1)\psi_1 - \mathcal{K}\psi_2 \tag{A10a}$$

$$i\hbar\frac{\partial\psi_2}{\partial t} = (E^0_2 + U_2N_2)\psi_2 - \mathcal{K}\psi_1. \tag{A10b}$$

Note that because of the GPE nonlinearity, the parmeters $U, \mathcal{K}, E^0$ are implicit functions of N_T, the atomic density.

APPENDIX B: REVIEW OF PROPERTIES OF ELLIPTIC FUNCTIONS

a. *Symmetric Wells:* Let us first look at the case $\Delta E = 0$. One writes the basic equation in the form given in Eq. (3.5),

$$\frac{\Lambda t}{2} = \int_{z(t)}^{z(0)} \frac{dz}{\sqrt{(\alpha^2 + z^2)(C^2 - z^2)}}, \tag{B1}$$

where

$$C^2 = \frac{2}{\Lambda^2}\left[(H_0\Lambda - 1) + \frac{\zeta^2}{2}\right] \; ; \; \alpha^2 = \frac{2}{\Lambda^2}\left[\zeta^2 - (H_0\Lambda - 1)\right], \tag{B2a}$$

$$\zeta^2(\Lambda) = 2\sqrt{\Lambda^2 + 1 - 2H_0\Lambda}. \tag{B2b}$$

The solution to that equation is given in terms of Jacobian elliptic functions,

$$\begin{aligned} z(t) &= C\mathrm{cn}[(C\Lambda/k)(t - t_0), k] \\ &= C\mathrm{dn}[(C\Lambda)(t - t_0), 1/k], \end{aligned} \tag{B3a}$$

$$k^2 = \frac{1}{2}\left(\frac{C\Lambda}{\zeta}\right)^2 = \frac{1}{2}\left[1 + \frac{(H_0\Lambda - 1)}{\sqrt{\Lambda^2 + 1 - 2H_0\Lambda}}\right], \tag{B3b}$$

$$t_0 = 2[\Lambda\sqrt{C^2 + \alpha^2}F(\arccos(z(0)/C), k)]^{-1} \tag{B3c}$$

where C, α are defined in Eq. (B2b), $F(\phi, k) = \int_0^\phi d\varphi(1 - k^2\sin^2\varphi)^{-1/2}$ is the incomplete elliptic integral of the first kind and the functions cn and dn are the Jacobian elliptic functions with k as the elliptic modulus defined in Eq. (B3b). The key quantity governing the behavior of the elliptic functions is the elliptic modulus k (or the elliptic parameter k^2). When $0 < k^2 < 1$, the function is usually written in terms of the cn function. Further, when $k^2 \ll 1$, it takes approximate forms given by

$$\mathrm{cn}(u, k) \approx \cos u + k^2(\sin u)(u - \sin(2u)/2). \tag{B4}$$

However, when k increases, the departure from these simple trigonometric forms is more drastic. Specifically, when $k \lesssim 1$, the approximate form is

$$\mathrm{cn}(u, k) \approx \mathrm{sech}u - (1 - k^2)(\tanh u\mathrm{sech}u)(\sinh u\cosh u - u)/4. \tag{B5}$$

When $k^2 = 1$, the cn function takes the hyperbolic secant form. When $k^2 > 1$, the natural function is the dn function, and once $k^2 \gg 1$, it takes trigonometric approximations once more,

$$\mathrm{dn}(u, 1/k) \approx 1 - \sin^2 u/2k^2. \tag{B6}$$

The elliptic functions cn and dn are periodic with a period given by $4K(k), 2K(1/k)$ respectively where $K(k)$ is the complete elliptic integral of the first kind. Specifically, as $k \to 1$, the time period diverges logarithmically, $\lim_{k\to 1} K(k) = \log(4/\sqrt{1 - k^2})$. For $k \to 0$, $K(k) \to \pi/2$.

b. *Asymmetric Wells*: For the case $\Delta E \neq 0$, one obtains Eq. (4.1),

$$\frac{\Lambda t}{2} = \int_{z(t)}^{z(0)} \frac{dz'}{\sqrt{f(z')}}, \tag{B7a}$$

$$f(z) = \left(\frac{2}{\Lambda}\right)^2 (1 - z^2) - \left[z^2 + \frac{2z\Delta E}{\Lambda} - \frac{2H_0}{\Lambda}\right]^2 \tag{B7b}$$

One first writes the r.h.s. of Eq. (B7) as

$$\int_{z(t)}^{z(0)} \frac{dz'}{\sqrt{f(z')}} = \int_{z_1}^{z(0)} \frac{dz'}{\sqrt{f(z')}} + \int_{z(t)}^{z_1} \frac{dz'}{\sqrt{f(z')}}, \tag{B8}$$

where z_1 is a real root of $f(z)$. Defining the first term on the r.h.s of Eq. (B8) to be $\Lambda t_0/2$, we are faced with the evaluation of the second term. In the method below, we shall follow Ref. [44] closely. Recognizing that $f(z_1) = 0$, we expand $f(z)$ about z_1. We, further, define

$$\sigma = \nu f'(z_1)/4 + f''(z_1)/24 \; ; \; s = \xi f'(z_1)/4 + f''(z_1)/24, \tag{B9a}$$

$$\xi = 1/(z' - z_1) \; ; \; \nu = 1/(z - z_1) \tag{B9b}$$

and rewrite Eq. (B7) as

$$\frac{\Lambda(t - t_0)}{2} = \int_s^\infty \frac{d\nu}{\sqrt{4\sigma^3 - g_2\sigma - g_3}}, \tag{B10}$$

where

$$g_2 = -a_4 - 4a_1a_3 + 3a_2^2 \; ; \; g_3 = -a_2a_4 + 2a_1a_2a_3 - a_2^3 + a_3^2 - a_1^2a_4, \tag{B11a}$$

$$a_1 = -\frac{\Delta E}{\Lambda} \; ; \; a_2 = \frac{2}{3\Lambda^2}(\Lambda(H_0 + 1) - \Delta E^2) \; ; \; a_3 = \frac{2H_0\Delta E}{\Lambda^2} \; ; \; a_4 = \frac{4(1 - H_0^2)}{\Lambda^2}. \tag{B11b}$$

Equation (B10) can be inverted immediately to give the solution of s as a function of t in terms of Weierstrassian elliptic functions. One thus obtains Eq. (4.2)

$$z(t) = z_1 + \frac{6f'(z_1)}{24\wp(\Lambda(t - t_0)/2; g_2, g_3) - f''(z_1)}, \tag{B12}$$

where the constant t_0 is given below. From Eq. (B10) we have

$$\frac{\Lambda t_0}{2} = -\int_s^\infty \frac{d\mu}{\sqrt{4\eta^3 - g_2\eta - g_3}}, \tag{B13}$$

where

$$\eta = \mu f'(z_1)/4 + f''(z_1)/24 \; ; \; \mu = 1/(z(0) - z_1). \tag{B14}$$

One then explicitly writes the denominator of Eq. (B13) in terms of its roots as

$$4x^3 - g_2 x - g_3 = 0 = 4(x - e_1)(x - e_2)(x - e_3). \tag{B15}$$

Combining Eqs. (B13),(B15), one obtains

$$\Lambda t_0 = -\frac{2}{\sqrt{e_1 - e_3}} F(\varphi, k), \tag{B16}$$

where $\varphi = \arcsin\sqrt{(e_1 - e_3)(s - e_3)}$ and k is the elliptic parameter whose specific forms are given below as appropriate arguments of the Jacobian functions [see, e.g., Eqs. (B19),(B21).] To arrive at the properties of the Weierstrassian elliptic function itself, one begins by constructing the discriminant

$$\delta = g_2^3 - 27 g_3^2. \tag{B17}$$

If $\delta > 0$, all the roots e_i in Eq. (B15) are real and are given by

$$e_1 = -\sqrt{g_2/3}\cos\left(\frac{\theta}{3}\right), \tag{B18a}$$

$$e_2 = -\sqrt{g_2/3}\cos\left(\frac{\theta + 2\pi}{3}\right), \tag{B18b}$$

$$e_3 = -\sqrt{g_2/3}\cos\left(\frac{\theta - 2\pi}{3}\right), \tag{B18c}$$

$$\theta = \arccos(\sqrt{27 g_3^2/g_2^3}). \tag{B18d}$$

Then the Weierstrassian elliptic function takes the form

$$\wp(y) = e_3 + \frac{e_1 - e_3}{\mathrm{sn}^2(y\sqrt{e1 - e3}, k_1)}, \tag{B19a}$$

$$k_1^2 = \frac{e_2 - e_3}{e_1 - e_3}. \tag{B19b}$$

Here sn refers to the Jacobian sn elliptic function. If $\delta < 0$, there are two complex conjugate roots and only one real root (denoted usually by e_2), and given by

$$e_2 = \frac{1}{2}\left[(g_3 + \sqrt{-\delta/27})^{1/3} + (g_3 - \sqrt{-\delta/27})^{1/3}\right], \tag{B20a}$$

and the Weierstrassian elliptic function is given by

$$\wp(y) = e_2 + H_2 \frac{1 + \mathrm{cn}(2y\sqrt{H_2}, k_2)}{1 - \mathrm{cn}(2y\sqrt{H_2}, k_2)}, \tag{B21a}$$

$$H_2^2 = 3e_2^2 - g_2 \ , \ k_2^2 = \frac{1}{2} - \frac{3e_2}{4H_2}. \tag{B21b}$$

When the discriminant, δ, is zero, the Weierstrassian elliptic function takes on specific forms [34], as below:

$$\text{For } g_2 > 0 \ , \ g_3 < 0 \ , \ e_1 = e_2 = c, e_3 = -2c \ ; \ c = (1/2)|g_3|^{1/3} : \tag{B22a}$$

$$\wp(y) = \frac{|g_3|^{1/3}}{2} + \frac{3|g_3|^{1/3}}{2\sinh^2\left[\left(\frac{3|g_3|^{1/3}}{2}\right)^{1/2} y\right]}. \tag{B22b}$$

$$\text{For } g_2 > 0 \ , \ g_3 > 0 \ , \ e_1 = 2c, e_2 = e_3 = -c \ ; \ c = (1/2)|g_3|^{1/3} : \tag{B23a}$$

$$\wp(y) = -\frac{|g_3|^{1/3}}{2} + \frac{3|g_3|^{1/3}}{2\sin^2\left[\left(\frac{3|g_3|^{1/3}}{2}\right)^{1/2} y\right]}. \tag{B23b}$$

$$\text{For } g_2 = g_3 = e_1 = e_2 = e_3 = 0, \tag{B24a}$$

$$\wp(y) = 1/y^2. \tag{B24b}$$

Although the solutions have been written down in terms of the Jacobian elliptic, trigonometric, and hyperbolic functions in Eqs. (B19,B21a, B22,B23,B24), the fourier transforms are not susceptible to a closed form evaluation of the spectrum as was the case for the symmetric trap. However, it is still possible to calculate the time-period analytically in terms of the complete elliptic integral of the first kind [34]. We give below a brief listing of the explicit dependence of the time-period τ on the parameters of the problem,

$$\delta > 0 \ : \ \tau = K(k_1)/(e_1 - e_3), \tag{B25a}$$

$$\delta < 0 \ : \ \tau = K(k_2)/\sqrt{H_2}, \tag{B25b}$$

$$\delta = 0 \ , \ g_2 > 0, g_3 < 0 \ : \ \tau = \infty, \tag{B25c}$$

$$\delta = 0 \ , \ g_2 > 0, g_3 > 0 \ : \ \tau = \pi/\sqrt{6g_3^{1/3}}, \tag{B25d}$$

$$\delta = 0 \ , \ g_2 = g_3 = 0 \ : \ \tau = \infty, \tag{B25e}$$

where $K(k)$ is the complete elliptic integral of the first kind and $k_{1,2}, e_{1,2,3}, g_{2,3}$ are defined in Eqs. (4.2b, B22,B23,B24).

REFERENCES

[1] S. N. Bose, Z. Phys. **26**, 178 (1924).

[2] A. Einstein, Sitzber. Kgl. Akad. Wiss., (1924), p.261; (1925), p.3 . For a historical view, see also A. Pais, *Subtle is the Lord, The Science and the Life of Albert Einstein* (Clarendon Press, Oxford, 1982), Ch. 23.

[3] M. H. Anderson, M. R. Matthews, C. E. Wieman, and E. A. Cornell, Science **269**, 198 (1995).

[4] K. B. Davis, M.-O. Mewes, M. R. Andrews, N. J. van Druten, D. S. Durfee, D. M. Kurn, and W. Ketterle, Phys. Rev. Lett. **75**, 3969 (1995).

[5] C. C. Bradley, C. A. Sackett, J. J. Tollett, and R. G. Hulet, Phys. Rev. Lett. **75**, 1687 (1995).

[6] M. R. Andrews, C. G. Townsend, H.-J. Miesner, D. S. Durfee, D. M. Kurn, and W. Ketterle, Science **275**, 637 (1997).

[7] L. Solymar, *Superconductive tunnelling and applications* (Chapman and Hall, London, 1972).

[8] A. J. Dahm, A. Denenstein, T. F. Finnegan, D. N. Langenberg, and D. J. Scalapino, Phys. Rev. Lett. **20**, 859 (1968), and references therein.

[9] L. P. Pitaevskii, Sov. Phys. JETP, **13**, 451 (1961); E. P. Gross, Nuovo Cimento **20**, 454 (1961); J. Math. Phys. **4**, 4704 (1963).

[10] S. Stringari, Phys. Rev. Lett. **77**, 2360 (1996).

[11] M. Edwards, P. A. Ruprecht, K. Burnett, R. J. Dodd, and C. W. Clark, Phys. Rev. Lett. **77**, 1671 (1996).

[12] A. Smerzi and S. Fantoni, Phys. Rev. Lett. **78**, 3589 (1997).

[13] Y. Kagan, E. L. Surkov, and G. V. Shlyapnikov, Phys. Rev. A **55**, R18 (1997).

[14] A. Smerzi, S. Fantoni, S. Giovannazzi, and S. R. Shenoy, Phys. Rev. Lett., submitted.

[15] V. M. Kenkre and D. K. Campbell, Phys. Rev. B **34**, 4959 (1986).

[16] M. W. Jack, M. J. Collett, and D. F. Walls, Phys. Rev. A **54**, R4625 (1996).

[17] A. Imamoğlu, M. Lewenstein, and L. You, Phys. Rev. Lett. **78**, 2511 (1997).

[18] M.-O. Mewes, M. R. Andrews, D. M. Kurn, D. S. Durfee, C. G. Townsend, and W. Ketterle, Phys. Rev. Lett. **78**, 582 (1997).

[19] P. W. Anderson, Rev. Mod. Phys. **38**, 298 (1969).

[20] O. Avenel and E. Varoquaux, Phys. Rev. Lett. **55**, 2704 (1985).

[21] P. Sokol, in *Bose-Einstein Condensation*, edited by A. Griffin, D. W. Snoke, and S. Stringari (Cambridge University Press, Cambridge, 1995), and references therein.

[22] B. D. Esry, C. H. Greene, J. P. Burke, Jr., and J. L. Bohn, Phys. Rev. Lett. **78**, 3594 (1997).

[23] V. M. Kenkre and G. P. Tsironis, Phys. Rev. B **35**, 1473 (1987).

[24] J. D. Andersen and V. M. Kenkre, Phys. Rev. B **47**, 11134 (1993).

[25] V. M. Kenkre and M. Kuś, Phys. Rev. B **46**, 13792 (1992).

[26] S. Raghavan, V. M. Kenkre, and A. R. Bishop, to appear in Phys. Lett. A.

[27] G. P. Tsironis and V. M. Kenkre, Phys. Lett. A **127**, 209 (1988).

[28] V. M. Kenkre, in *Singular Behavior and Nonlinear Dynamics*, edited by S. Pnevmatikos, T. Bountis, and S. Pnevmatikos (World Scientific, Singapore, 1989).

[29] G. P. Tsironis, Ph.D. thesis, University of Rochester, 1986, (unpublished).

[30] P. F. Byrd and M. D. Friedman, *Handbook of elliptic integrals for engineers and scientists, 2nd ed.* (Springer, Berlin, 1971).

[31] L. M. Milne-Thomson, in *Handbook of Mathematical Functions*, edited by M. Abramowitz and I. A. Stegun (Dover, New York, 1970).

[32] J. Javanainen, Phys. Rev. Lett. **57**, 3164 (1986).

[33] J. Ruostekoski and D. Walls, preprint cond-mat/9703190.

[34] T. H. Southard, in *Handbook of Mathematical Functions*, edited by M. Abramowitz and I. A. Stegun (Dover, New York, 1970).

[35] D. H. Dunlap and V. M. Kenkre, Phys. Rev. B **34**, 3625 (1986).

[36] D. H. Dunlap and V. M. Kenkre, Phys. Lett. A **127**, 438 (1988).

[37] D. H. Dunlap and V. M. Kenkre, Phys. Rev. B **37**, 6622 (1988).

[38] S. Raghavan, V. M. Kenkre, D. H. Dunlap, A. R. Bishop, and M. I. Salkola, Phys. Rev. A **54**, R1781 (1996).

[39] G. S. Agarwal and W. Harshawardhan, Phys. Rev. A **50**, R4465 (1994).

[40] P. Nozières and D. Pines, *The Theory of Quantum Fluids* (Addison-Wesley, Redwood City, California, 1990), Vol. II.

[41] V. V. Goldman, I. F. Silvera, and A. J. Leggett, Phys. Rev. B **24**, 2870 (1981).

[42] See e.g., V. V. Tolmachev, Dokl. Akad. Nauk SSR, **134**, 1324 (1960) [Sov. Phys. Dokl. **5**, 984 (1960)].

[43] S. Giorgini, L. P. Pitaevskii, and S. Stringari, preprint condmat/970414.

[44] E. T. Whittaker and G. N. Watson, *A Course of Modern Analysis*, fourth ed. (Cambridge University Press, Cambridge, 1969).

FIGURES

FIG. 1. The double well trap for two Bose-Einstein condensates with $N_{1,2}$ and $E^0_{1,2}$, the number of particles and the zero-point energies in the traps 1 and 2 respectively.

FIG. 2. Population imbalance $z(t)$ as a function of dimensionless time, with initial conditions $z(0) = 0.6, \phi(0) = 0$, symmetric trap, and nonlinearity parameters Λ as shown.

FIG. 3. τ_p/τ as a function of Λ/Λ_c (see text for definitions) and $z(0)$ values as shown. Dotted (dashed) line refers to $\phi(0) = 0(\pi)$. The inset of (a) shows the time-averaged value $\langle z(t)\rangle$ plotted against Λ/Λ_c.

FIG. 4. The time-fourier transform $z(\omega)$ of $z(t)$ as a function of the dimensionless frequency ω/Λ and Λ/Λ_c values as shown, $z(0) = 0.1$ and symmetric trap. The dotted (dashed) lines refer to $\phi(0) = 0(\pi)$.

FIG. 5. τ_{ac}/τ plotted against Λ for asymmetric trap parameter $\Delta E = 1$. In the main figure, the solid (dashed) line denotes $\phi(0) = 0(\pi)$. The vertical scale on the left (right) corresponds to the initial condition $\phi(0) = 0(\pi)$. The insets show time-averaged $\langle z\rangle$ against Λ, for (a), $\phi(0) = \pi$ and (b), $\phi(0) = 0$.

FIG. 6. τ_{ac}/τ plotted against trap asymmetry parameter ΔE for various values of Λ/Λ_c. See text for definition for τ_{ac}. $z(0) = 0.1$. In (a), $\phi(0) = 0$ and in (b), $\phi(0) = \pi$.

FIG. 7. Analog of Shapiro effect: dc current $I_{dc} = \langle \dot{z}\rangle$ as a function of trap asymmetry parameter scaled in applied frequency, $\Delta E/\omega_0$, for various values of Λ as shown.

FIG. 8. Theoretical inverse periods cast in a form suitable for direct experimental comparison. See text, Section VI.

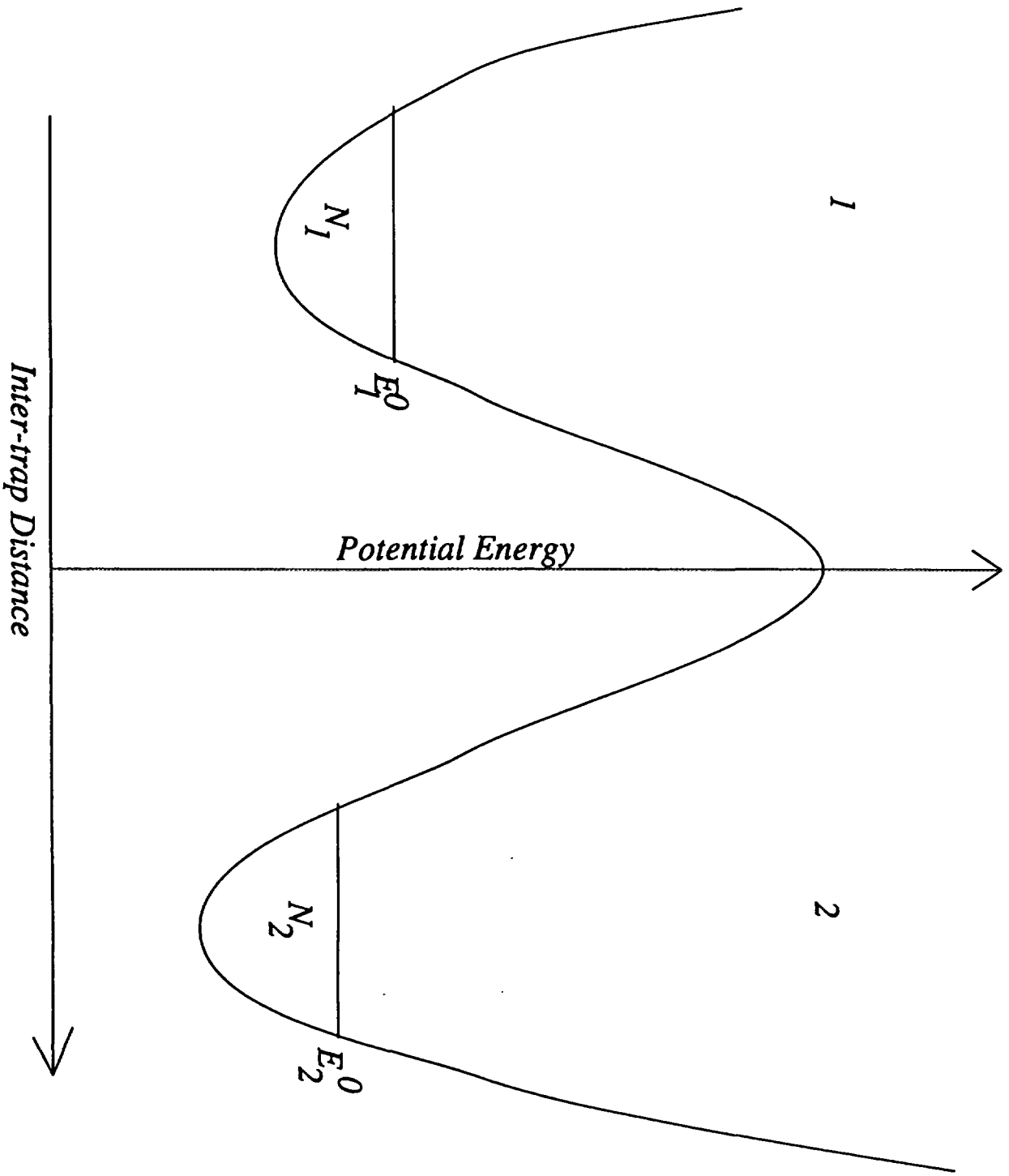

Fig. 1

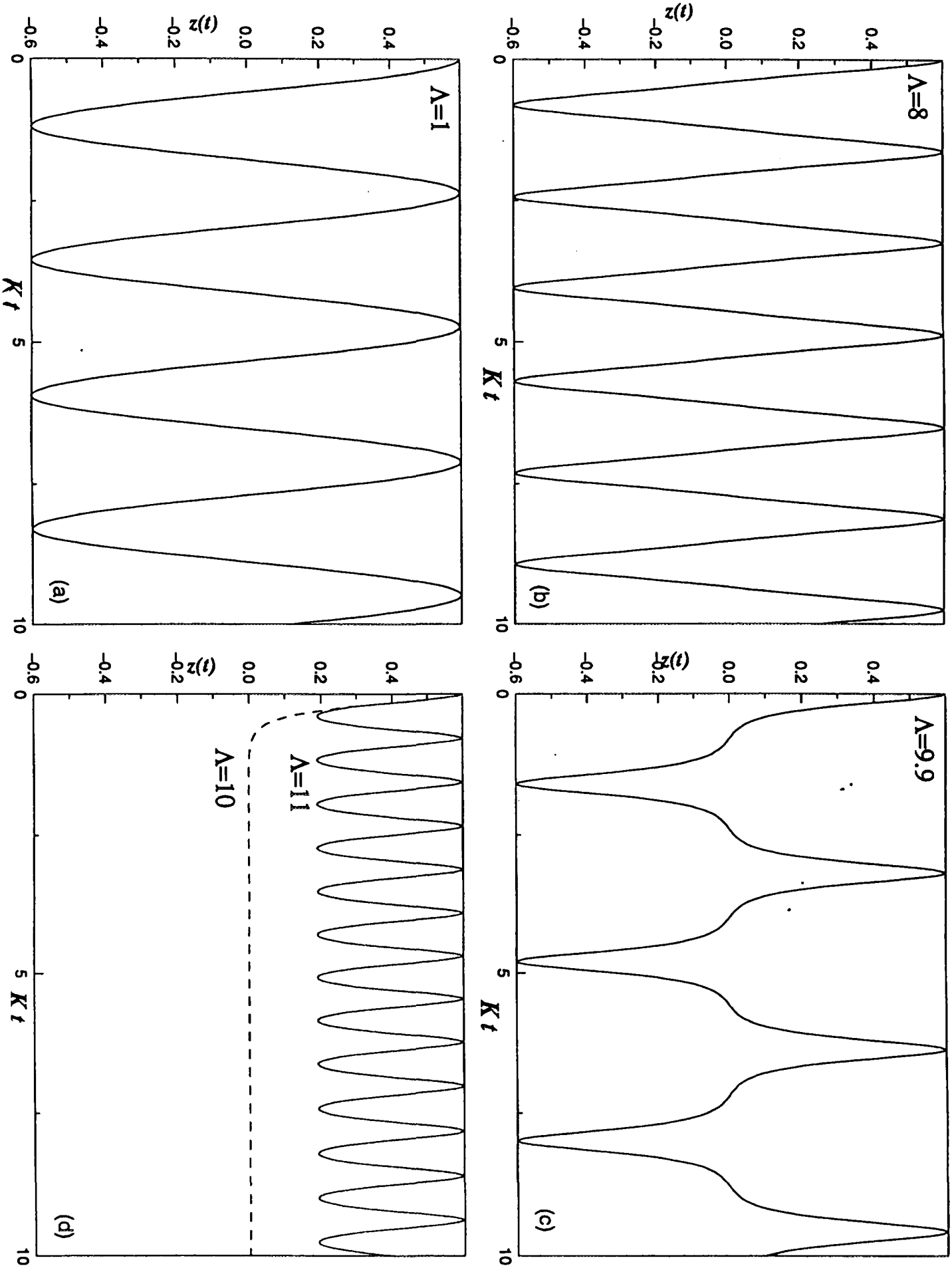

Fig.2

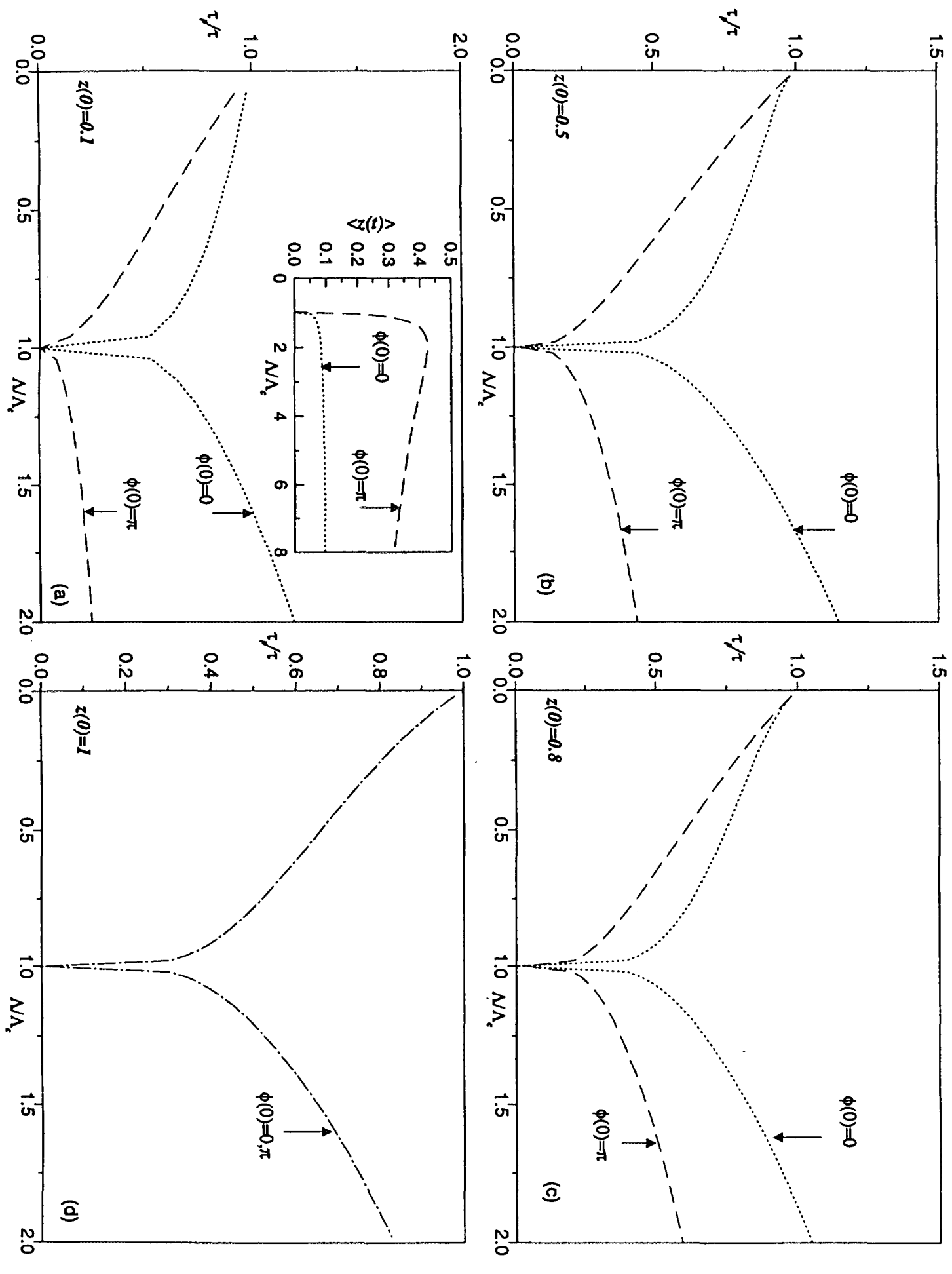
z(0)=0.1
(a)
φ(0)=0
φ(0)=π
<z(t)>
φ(0)=0
φ(0)=π
z(0)=0.5
(b)
φ(0)=0
φ(0)=π
z(0)=0.8
(c)
φ(0)=0
φ(0)=π
z(0)=1
(d)
φ(0)=0,π
τ/τ
Λ/Λ_ε

Fig.3

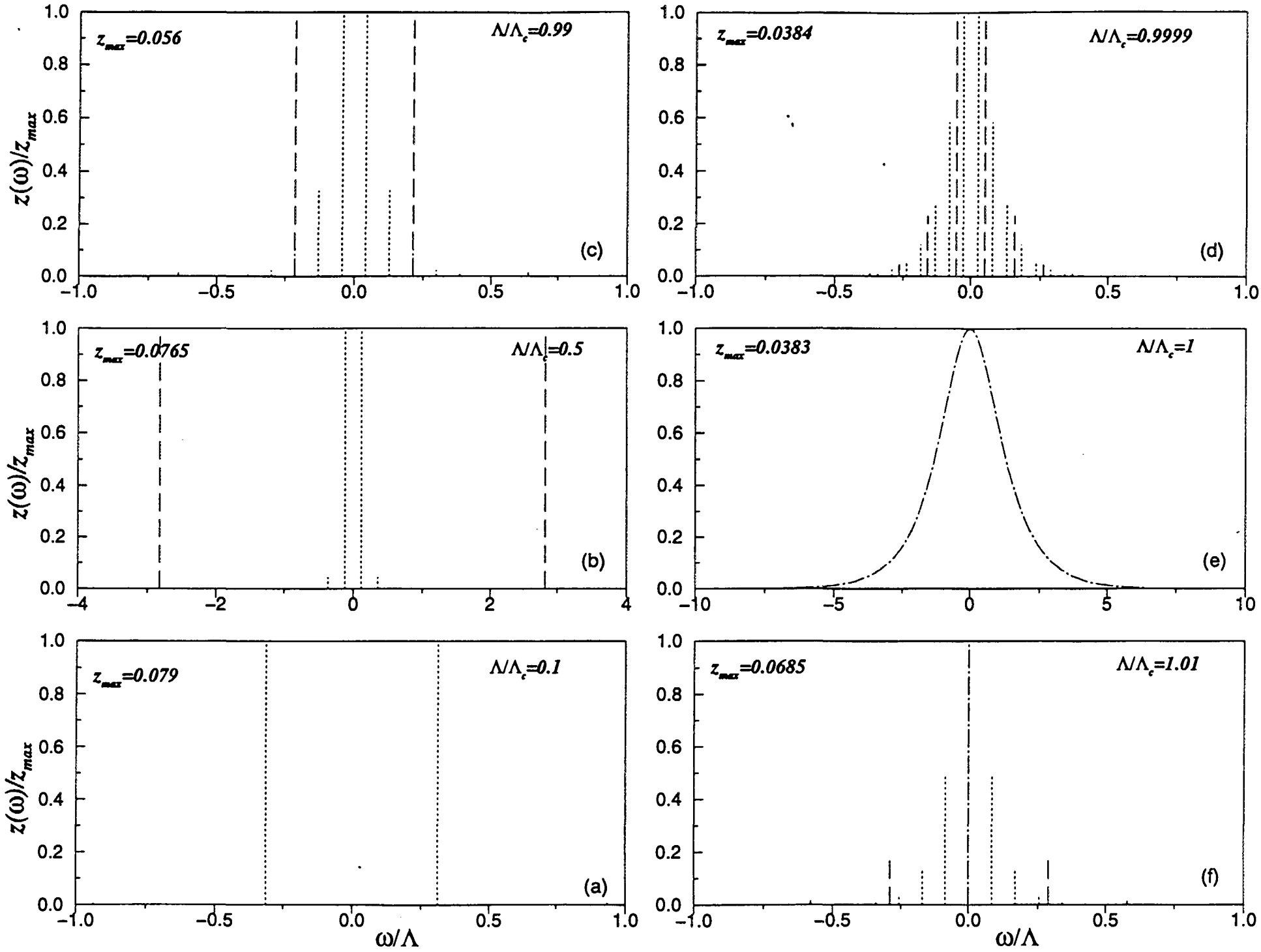
z_{max}=0.056
Λ/Λ_c=0.99
(c)
z_{max}=0.0384
Λ/Λ_c=0.9999
(d)
z_{max}=0.0765
Λ/Λ_c=0.5
(b)
z_{max}=0.0383
Λ/Λ_c=1
(e)
z_{max}=0.079
Λ/Λ_c=0.1
(a)
z_{max}=0.0685
Λ/Λ_c=1.01
(f)
$z(\omega)/z_{max}$
ω/Λ

Fig. 4

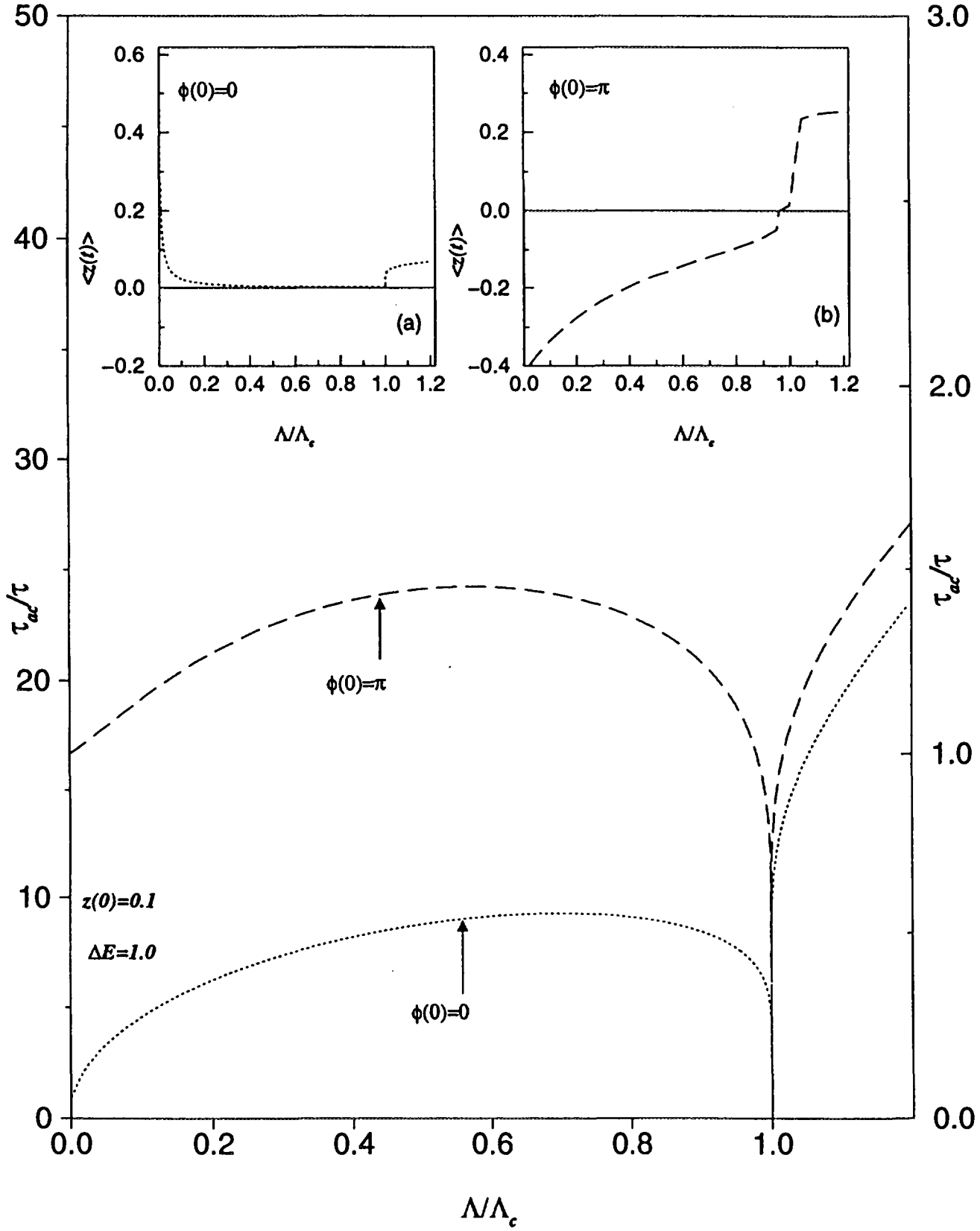
50
40
30
20
10
0
3.0
2.0
1.0
0.0
τ_{ac}/τ
0.0
0.2
0.4
0.6
0.8
1.0
Λ/Λ_c
$\phi(0)=\pi$
$\phi(0)=0$
z(0)=0.1
ΔE=1.0
0.6
0.4
0.2
0.0
−0.2
$\phi(0)=0$
(a)
$\langle z(t)\rangle$
0.0 0.2 0.4 0.6 0.8 1.0 1.2
Λ/Λ_c
0.4
0.2
0.0
−0.2
−0.4
$\phi(0)=\pi$
(b)
$\langle z(t)\rangle$
0.0 0.2 0.4 0.6 0.8 1.0 1.2
Λ/Λ_c

Fig. 5

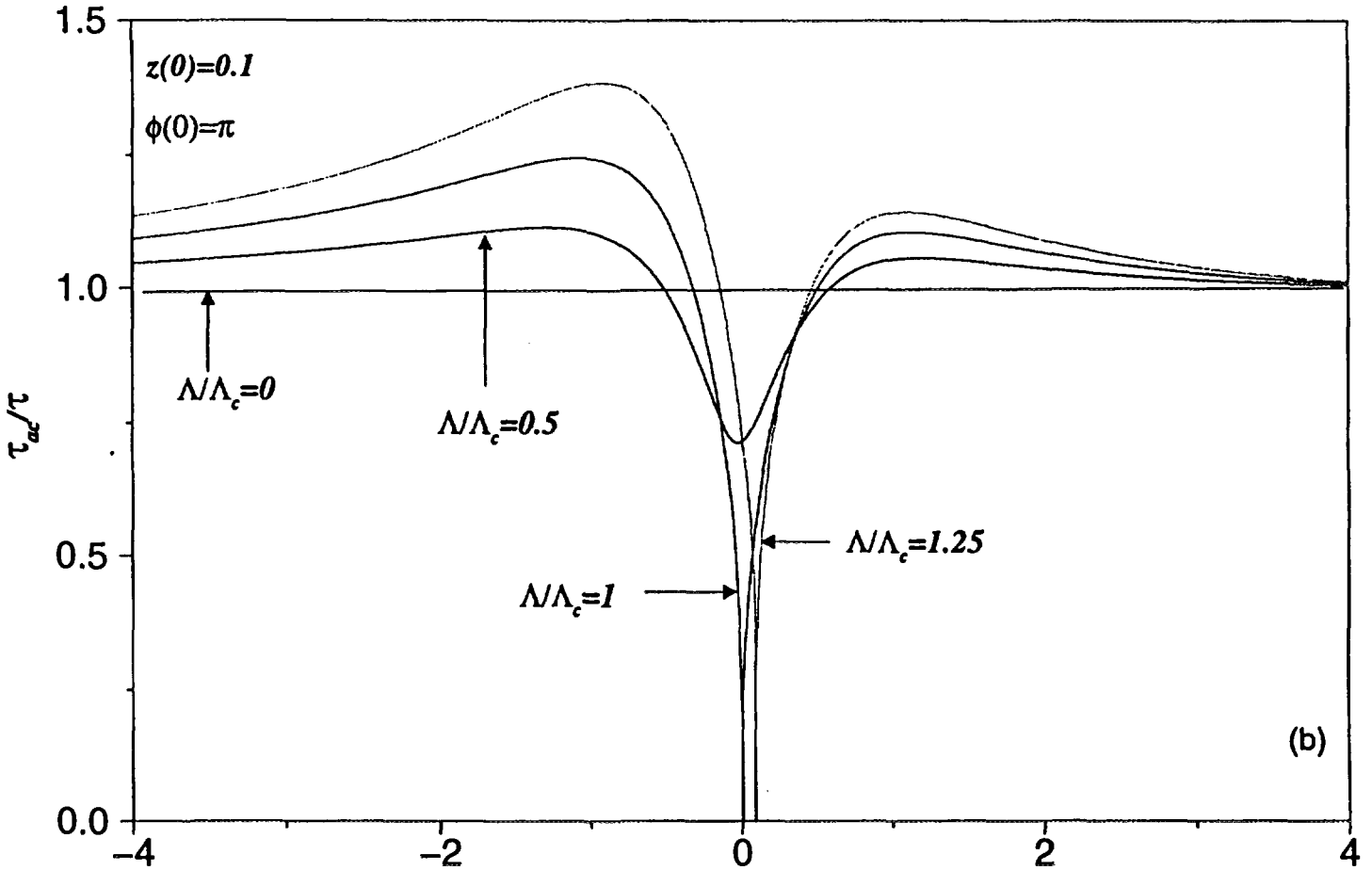
z(0)=0.1
φ(0)=π
Λ/Λc=0
Λ/Λc=0.5
Λ/Λc=1
Λ/Λc=1.25
τac/τ
(b)

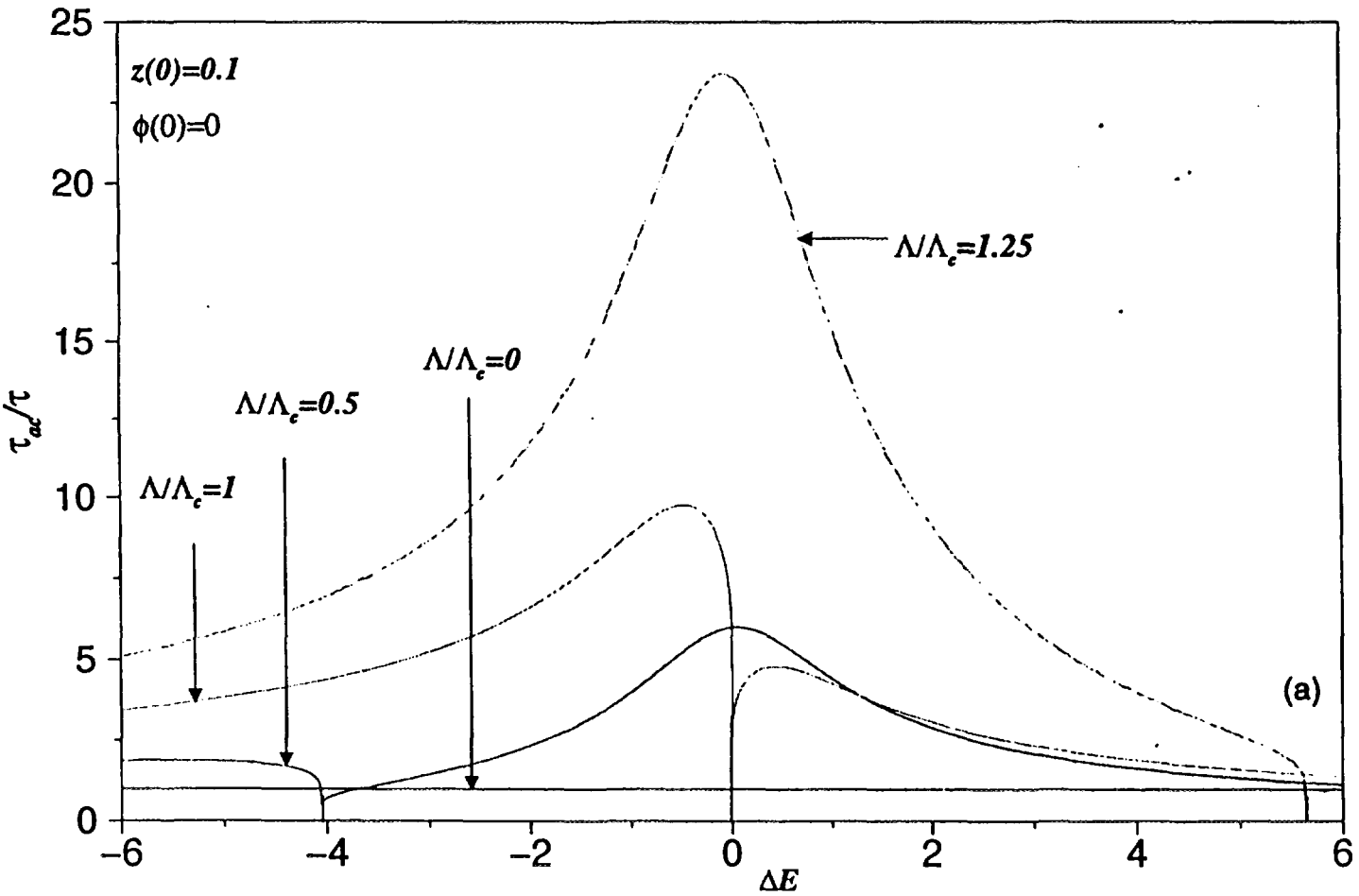
z(0)=0.1
φ(0)=0
Λ/Λc=1.25
Λ/Λc=0
Λ/Λc=0.5
Λ/Λc=1
τac/τ
ΔE
(a)

Fig. 6

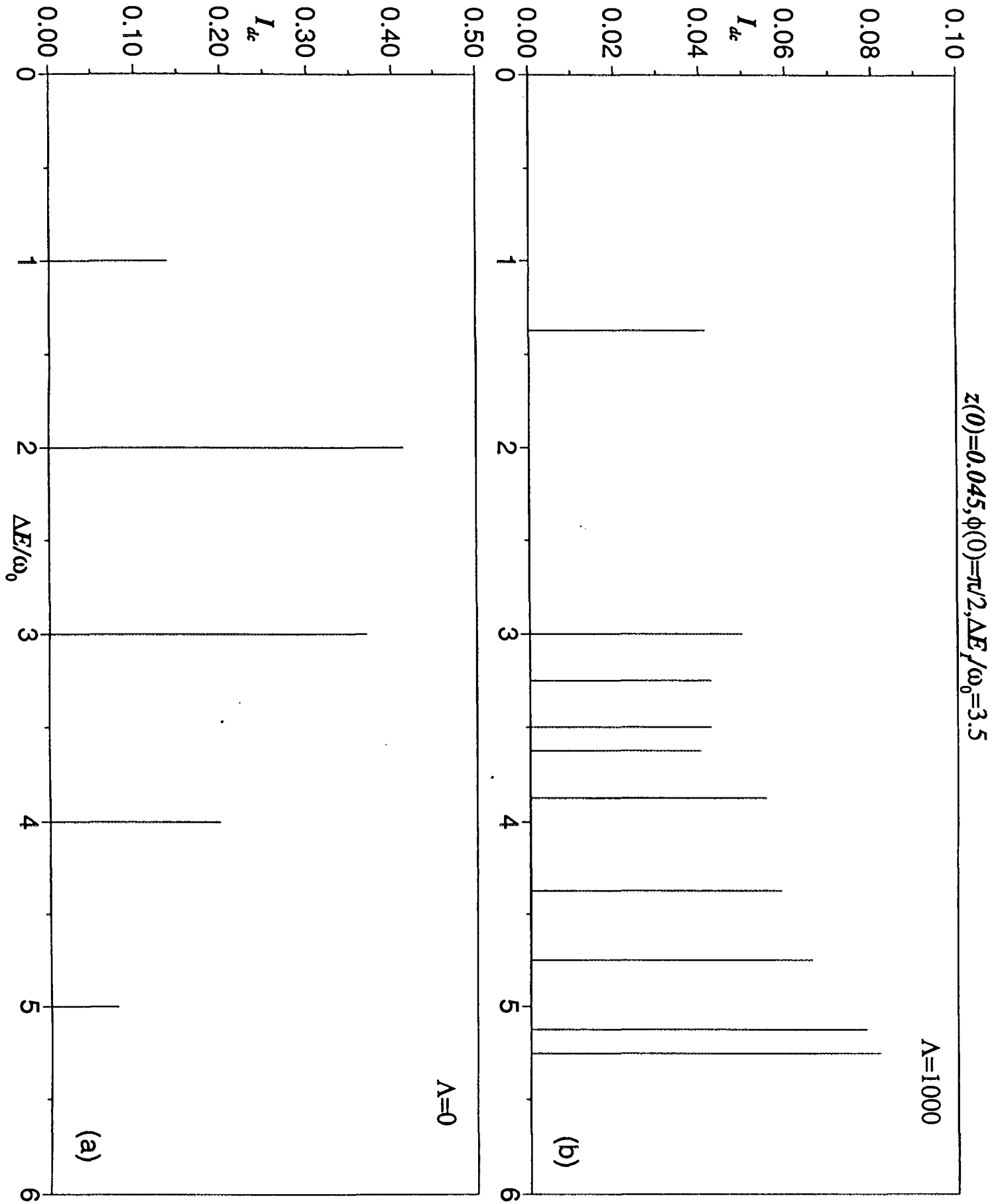
z(0)=0.045, φ(0)=π/2, ΔE_f/ω_0=3.5
(a)
Λ=0
(b)
Λ=1000
I_dc
ΔE/ω_0
0.00
0.10
0.20
0.30
0.40
0.50
0.02
0.04
0.06
0.08
0
1
2
3
4
5
6

Fig. 7

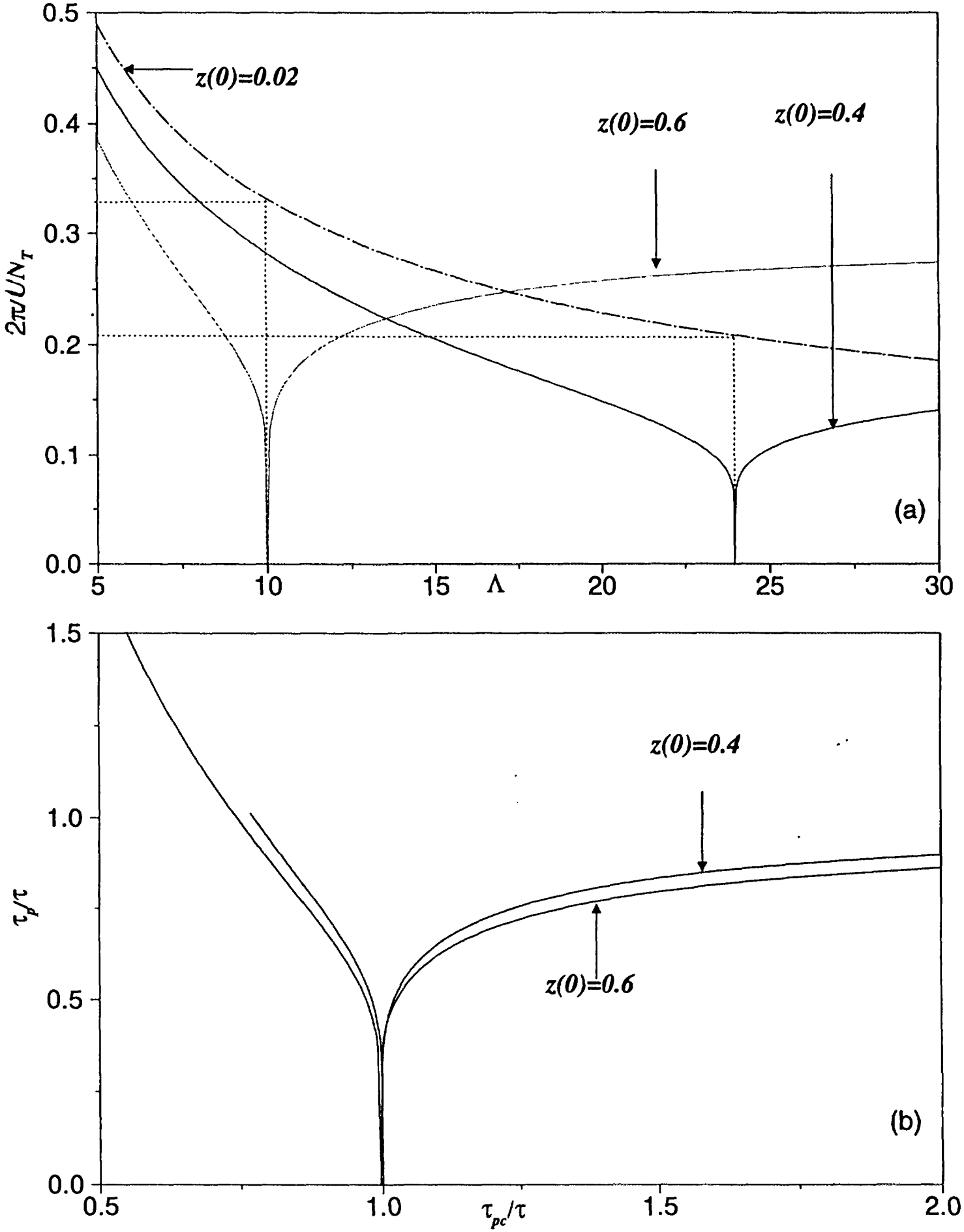
0.5
0.4
0.3
0.2
0.1
0.0
$2\pi/UN_T$
z(0)=0.02
z(0)=0.6
z(0)=0.4
(a)
5
10
15
Λ
20
25
30
1.5
1.0
0.5
0.0
τ_p/τ
z(0)=0.4
z(0)=0.6
(b)
0.5
1.0
τ_{pc}/τ
1.5
2.0

Fig. 8